EFFECTS OF MODIFICATIONS TO THE SPACE SHUTTLE ENTRY GUIDANCE AND CONTROL SYSTEMS

Richard W. Powell, Howard W. Stone, and Lawrence F. Rowell

Langley Research Center
Hampton, Va. 23665

1 Report No NASA TN D-8273	2 Government Accession No	3 Recipient's Catalog No	
4 Title and Subtitle EFFECTS OF MODIFICATIONS TO THE SPACE SHUTTLE ENTRY GUIDANCE AND CONTROL SYSTEMS		5 Report Date October 1976	
		6 Performing Organization Code	
7 Author(s) Richard W. Powell, Howard W. Stone, and Lawrence F. Rowell		8 Performing Organization Report No L-10408	
9 Performing Organization Name and Address NASA Langley Research Center Hampton, VA 23665		10 Work Unit No 506-26-30-01	
		11 Contract or Grant No	
		13 Type of Report and Period Covered Technical Note	
12 Sponsoring Agency Name and Address National Aeronautics and Space Administration Washington, DC 20546			
		14 Sponsoring Agency Code	

15 Supplementary Notes

16 Abstract

   A nonlinear six-degree-of-freedom entry simulation study was conducted to identify space shuttle orbiter guidance and control system software modifications which would reduce the control system sensitivity to the guidance system sampling frequency. Several modifications which eliminated the control system sensitivity and associated control limit cycling were examined; the result of the modifications was a reduction in required reaction control system fuel.

17 Key Words (Suggested by Author(s)) Space shuttle Entry guidance system Entry control system	18 Distribution Statement Unclassified - Unlimited Subject Category 15		
19 Security Classif (of this report) Unclassified	20 Security Classif (of this page) Unclassified	21 No of Pages 84	22 Price* $4.75

EFFECTS OF MODIFICATIONS TO THE SPACE SHUTTLE
ENTRY GUIDANCE AND CONTROL SYSTEMS

Richard W. Powell, Howard W. Stone,
and Lawrence F. Rowell
Langley Research Center

SUMMARY

A study was conducted using a nonlinear six-degree-of-freedom
digital simulator to identify modifications which would reduce the
space shuttle orbiter control system sensitivity to guidance sys-
tem sampling frequency and would eliminate limit cycling of the
controls. Previous nonlinear three-degree-of-freedom trajectory
analyses indicated that entry guidance requirements were satisfied
with attitude commands issued at 2-second intervals. Six-degree-
of-freedom analyses of the control system response to commands with
this long interval indicated that it resulted in limit cycling of
the reaction controls and, consequently, required large increases
in reaction control system fuel. A combination of control system
software modifications (a "ramp" designed to smooth the step sig-
nals to the control system together with gain modifications in
the yaw and the aileron control circuits) was identified that
eliminated the limit cycling and the sensitivity to guidance
sampling frequency. This combination resulted in a 64-percent
savings in reaction control system fuel during a nominal entry.

INTRODUCTION

A reusable Earth-to-orbit transportation system known as the
space shuttle is being developed under contract to the National
Aeronautics and Space Administration (NASA). The space shuttle is

to be capable of inserting payloads of up to 29 500 kg (65 000 lb) into a near-Earth orbit, retrieving payloads already in orbit, and landing with a payload of up to 14 500 kg (32 000 lb). The space shuttle consists of an orbiter, an external fuel tank, and two solid rocket boosters (SRB). The SRB's are to be recovered after launch for reuse. The external tank is designed for one use and is not recovered. The orbiter is to have the capability to reenter the atmosphere of the Earth, to fly up to 2040 km (1100 n. mi.) crossrange, and to land horizontally. A general description of the configuration and mission is given in reference 1.

The space shuttle orbiter can be automatically guided and controlled from entry to landing by onboard digital computers in conjunction with navigation, guidance, and flight control systems. The guidance system calculates the vehicle attitudes required to meet the targeting requirements without violating any in-flight constraints. The control system directs the aerodynamic surfaces (elevons, rudder, speed brake, and body flap) and the reaction control system (RCS) thrusters.

To maintain proper control, the control system is sampled at the minimum pulse width of the RCS thrusters, i.e., 0.04 second. However, it is not necessary to sample the guidance system so frequently, and from a computer burden standpoint, it is desirable to make the time between samples as long as possible. Previous three-degree-of-freedom nonlinear analyses of the entry have shown that a guidance sampling rate of once every 2.00 seconds is adequate to meet the targeting and in-flight constraints. However, six-degree-of-freedom simulations indicated that this lower frequency results in limit cycling in the RCS.

Four software modifications (developed in cooperation with E. E. Smith, Jr., and J. H. Suddath of the NASA Johnson Space Center, Houston, Texas) to the guidance and control systems are proposed to eliminate the limit cycling and accompanying fuel increase at the longer guidance intervals. This paper presents results of a study of the longer guidance intervals with the nominal systems and the effects of adding the proposed modifications.

2

SYMBOLS

Values are given in both SI and U.S. Customary Units.
The measurements were made in U.S. Customary Units. Symbols
used in the appendixes are defined therein.

dt   time between guidance system samplings, sec

E_Y yaw RCS error signal

E1   signal in yaw RCS control circuit

g   acceleration of gravity, m/sec^2 (ft/sec^2)

M   Mach number

p   roll rate about body axis, deg/sec

q   pitch rate about body axis, deg/sec

$\bar{q}$ dynamic pressure, Pa (psf)

r   yaw rate about body axis, deg/sec

r' $= r - \dfrac{180g \sin \phi \cos \theta}{\pi V}$, deg/sec

t   current trajectory time, sec

t_{guide} time of last guidance sampling, sec

V   Earth relative velocity, m/sec (ft/sec)

y_{cg} lateral center-of-gravity offset, m (ft)

α angle of attack, deg

α_c commanded angle of attack sent to control system, deg

$\alpha_{c,new}$ commanded angle of attack from guidance system at latest sampling, deg

$\alpha_{c,old}$ commanded angle of attack from guidance system at previous sampling, deg

β sideslip angle, deg

δ_a aileron deflection angle, deg

$\delta_{a,UD}$ commanded aileron deflection from up-down counter, deg

δ_{BF} body-flap deflection angle, deg

δ_e elevator deflection angle, deg

δ_r rudder deflection angle, deg

δ_{SB} speed-brake deflection angle, deg

θ pitch angle about body axis, deg

ϕ roll angle about body axis, deg

ϕ_c commanded roll angle about body axis sent to control system, deg

$\phi_{c,new}$ commanded roll angle from guidance system at latest sampling, deg

4

$\phi_{c,old}$ commanded roll angle from guidance system at previous sampling, deg

ϕ_{err} roll-error signal in control system $(\phi_c - \phi)$, deg

SPACE SHUTTLE ORBITER DESCRIPTION

The physical characteristics of the space shuttle orbiter discussed in this paper are summarized in table I. A sketch of the space shuttle orbiter indicating the aerodynamic controls and RCS location is shown in figure 1. The set of nominal aerodynamic characteristics is the June 1974 aerodynamic data base compiled by the contractor. The guidance and control schemes utilized in this study are described in appendixes A and B, respectively. The guidance and control schemes are applicable from deorbit to the terminal area energy management (TAEM) interface which occurs approximately 1880 seconds after deorbit. At this interface, the space shuttle orbiter is traveling at a velocity of 457.2 m/sec (1500 fps), and at an altitude of 21.3 km (70 000 ft).

The entry in the automatic mode is directed entirely by onboard computers. The guidance system software produces a series of angle-of-attack and roll-attitude commands which the control system software uses to direct the RCS and surface deflections.

AUTOMATIC REENTRY FLIGHT DYNAMICS SIMULATOR (ARFDS) DESCRIPTION

The guidance and control modifications were analyzed with the aid of the ARFDS. This program is an NASA Langley Research Center developed, nonlinear, six-degree-of-freedom, interactive, digital computer program which uses hardware developed for real-time simulations. The ARFDS includes an oblate rotating Earth model and uses nonlinear aerodynamics. The ARFDS is run from a control console where, at any time during the entry, control or guidance gains can be modified, winds or other disturbances added or removed, and guidance sampling frequency varied. However, no

5

winds or gusts were considered in this study. The entry states
can be observed on time-history strip charts, deficiencies can be
noted, and appropriate solutions can be incorporated.

MISSION DESCRIPTION

The space shuttle mission considered was a once-around return
that had been launched into a 104° inclined orbit from the Western
Test Range. This orbit results in a crossrange requirement of
2040 km (1100 n. mi.). Figure 2 shows some of the trajectory
parameters associated with this entry.

RESULTS AND DISCUSSION

Nominal Guidance and Control Systems Simulation Results

During the nominal entry, the guidance system issues step
commands to the control system at a predetermined rate. To deter-
mine the effect of varying this rate, the guidance sample time was
increased from 0.04 second (the control system sample time) to
2.00 seconds (the desired rate) in six steps.

Table II shows the fuel consumption associated with the
selected guidance sample times. Sampling times for the entire
entry between 0.04 and 0.64 second are within a fuel-consumption
range of 10 percent, whereas the 1.28- and 2.00-second times showed
fuel-consumption increases of 63 and 106 percent, respectively,
over that for the 0.04-second case. For the remainder of the
study, a 0.32-second sample time was used as typical of the shorter
times. Figure 3 shows the time histories of RCS fuel consumption
and roll angle ϕ for guidance sampling times of 0.32, 1.28, and
2.00 seconds, and figure 4 shows the corresponding simulation strip
charts for the entry between 300 and 500 seconds. The roll-angle
histories do not vary appreciably in these cases.

The shuttle is commanded to fly a roll angle of -15° until
approximately 400 seconds after deorbit. Between 400 and 500 sec-

6

onds, the angle increases to approximately -75°. During this period, there is a significant increase in RCS fuel consumption when the sampling time goes from 0.32 second to 1.28 seconds. There is a smaller increase between 1.28 seconds and 2.00 seconds (fig. 3). Alternate firings of both positive and negative yaw and roll jets, indicative of a control system limit cycle, occur for both the 1.28- and 2.00-second cases (figs. 4(b) and 4(c), respectively).

Limit cycling for the longer sampling times (1.28 and 2.00 sec) appears three more times in the trajectory. At approximately 1140 seconds into the entry, the guidance scheme changes from equilibrium glide to constant drag relationships to calculate ϕ_c. (See appendix A.) The constant drag relationships tend to produce wider variations in the ϕ_c signal; these variations result in limit cycling for the longer sampling times (shown by fig. 5 for a sampling time of 2.00 sec). At approximately 1500 seconds, the vehicle is commanded to perform a roll reversal. (The commanded roll angle ϕ_c changes signs.) At the end of the reversal, some limit cycling takes place again for the longer times (shown by fig. 6 for a sampling time of 2.00 sec). At a velocity of 2316 m/sec (7600 fps), which occurs at approximately 1550 seconds into the entry, additional guidance changes produce limit cycling (fig. 6). Figure 3 shows that during each of these periods of limit cycling of the roll and yaw jets, there is a corresponding increase in RCS fuel consumption that indicates that this limit cycling is the primary cause of the marked increase in fuel consumption. The control system changes to a more conventional aileron-rudder mode at approximately 1715 seconds and *no further* limit cycling is noted.

Modified Guidance and Control Systems Simulation Results

Four modifications designed to alleviate the RCS limit cycling associated with lower guidance sampling frequencies were examined. The first, designated "ramp," reduces the amplitude

of the step signal to the control system. The second modification, designated "gain," reduces the roll-rate response to small changes in ϕ_{err} by changing a gain in the yaw RCS circuit. "Up-down gain," the third modification, reduces the amount of aileron incremented by the up-down counter. Both gain and up-down gain provide improvements even for the more frequent guidance samplings. The fourth, "hysteresis," modifies the deadband filter in the ϕ_{err} signal of the yaw RCS circuit to a hysteresis type deadband filter.

Ramp smooths the guidance system roll angle and angle-of-attack signals by dividing the guidance step commands into small increments. The commanded roll angle ϕ_c used by the control system is calculated as follows:

$$\phi_c = \phi_{c,old} + \left(\frac{\phi_{c,new} - \phi_{c,old}}{dt}\right)(t - t_{guide})$$

The commanded angle-of-attack signal α_c is determined similarly. Thus, ϕ_c and α_c are varied between samplings as illustrated in sketch (a):
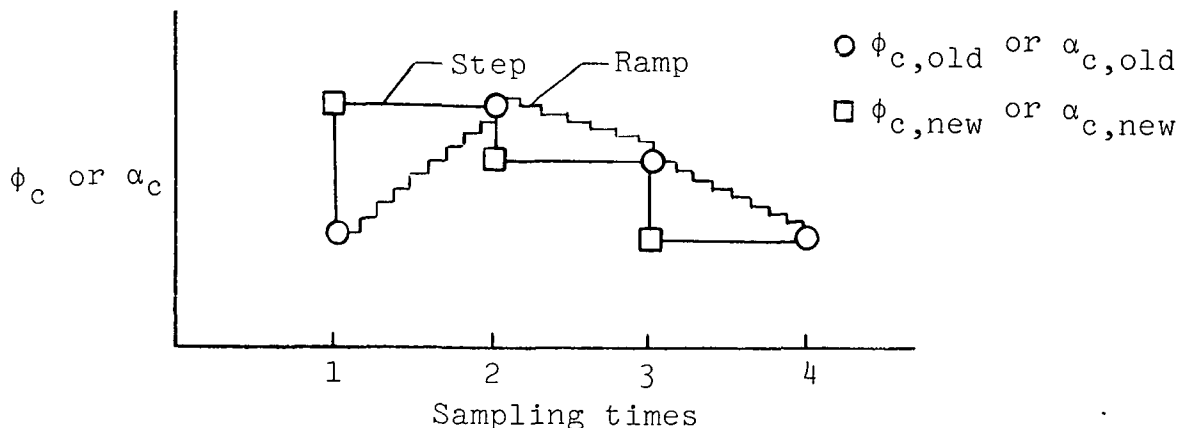
Sketch (a)

The smoothing action of ramp tended to eliminate the limit cycling of the roll and yaw RCS as shown by comparing figures 4(c) and 6 with 7(a) and 7(b), respectively.

8

Gain reduces the commanded roll rate for small changes in ϕ_{err} by multiplying E1 in the yaw RCS circuit (fig. 8) by three for $3^\circ < |\phi_{err}| < 17^\circ$. The value of ϕ_{err} is the difference between the commanded roll angle ϕ_c and the actual roll angle $\phi (\phi_{err} = \phi_c - \phi)$. Figure 9 shows the effects of gain for a commanded roll angle change of 10° for typical points along the trajectory. Gain reduces the roll-rate response to small values of ϕ_{err}. The strip charts of the entry with this modification (fig. 10) show that limit cycling is still present. A comparison of figures 4(c) and 10(a) shows that the amplitude of the roll rate and aileron oscillations and the duration of the yaw RCS cycling are somewhat reduced.

Up-down gain reduces the sensitivity of the $\delta_{a,UD}$ circuit to 40 percent of the nominal (fig. 11). The up-down counter calculates the aileron deflection $\delta_{a,UD}$ necessary to correct for the induced β caused by y_{cg} offsets and disturbances such as winds. Since the induced β will bias the firings, the up-down counter can be used to find an appropriate aileron deflection for lateral trim $\delta_{a,UD}$. This modification was designed to reduce fuel consumption caused by overtrimming by the ailerons; the time histories indicated there was no effect on the limit cycling.

Hysteresis was designed to prevent continued cycling of the yaw RCS about the deadband limit of the ϕ_{err} portion of the yaw RCS circuit. The ϕ_{err} portion of the yaw RCS circuit (fig. 8) was modified by introducing a hysteresis loop shown in sketch (b).
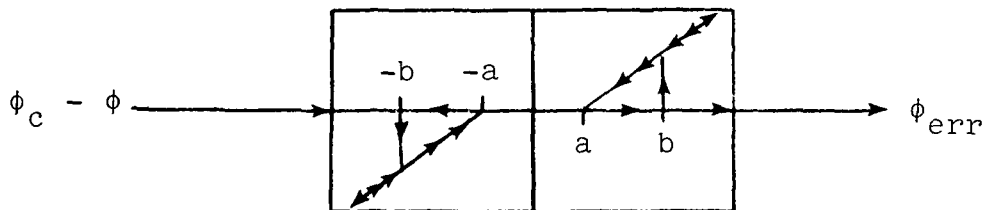
Sketch (b)

As the quantity $(\phi_c - \phi)$ increases from zero, ϕ_{err} remains zero until $\phi_c - \phi$ equals some preset value b. At this time, ϕ_{err} becomes $\phi_c - \phi - a$, where a is a preset value and remains equal

to this function as $\phi_c - \phi$ continues to increase. When $\phi_c - \phi$ decreases, ϕ_{err} continues to remain equal to $\phi_c - \phi - a$ until it becomes zero at $\phi_c - \phi = a$, and remains zero until $\phi_c - \phi$ equals b again. A similar relationship for ϕ_{err} occurs for negative values of $\phi_c - \phi$. Two sets of a's and b's were tried (a = 1.5, b = 3.0, and a = 3.0 and b = 4.5). Both sets tended to decrease the limit cycling slightly, but an a = 1.5 increased the total jet firing as the system activity increased because of the tighter deadband. For b = 4.5, large values of ϕ_{err} caused some increased jet firing as higher rates were commanded when jet firing was initiated.

The results of the simulations are summarized in table III and figure 12. The roll-angle time history shown in figure 12 is typical for all the simulations conducted. The data in this figure show that the most effective modifications were ramp and gain. Up-down gain showed negligible improvement, whereas hysteresis indicated an increase in fuel consumption. A combination of ramp with gain resulted in additional improvement in RCS fuel consumption over either modification alone (table III), and the addition of up-down gain improved the combined system resulting in a 64-percent reduction in total fuel requirement for a sampling frequency of 2.00 seconds.

To determine the effect of y_{cg} offsets, two combinations of these modifications were examined with the maximum expected offset of 0.038 m (1.5 in.). The two combinations were ramp with gain and ramp together with gain and up-down gain. The system with up-down gain still provided the smallest fuel consumption (table III) and required only 5.7 kg (12.5 lb) or 4 percent more fuel to handle the y_{cg} offset for the entire entry with a 2.00-second sampling time.

CONCLUDING REMARKS

A six-degree-of-freedom simulation study was conducted to identify space shuttle orbiter guidance and control system modifications

10

which would reduce the system sensitivity to guidance system sampling frequency and would eliminate limit cycling of the controls. Previous nonlinear three-degree-of-freedom trajectory analyses indicated that a guidance sampling rate of once every 2.00 seconds is adequate to meet the targeting and in-flight constraints. However, six-degree-of-freedom analyses of the control system response to commands at this long interval indicated that it resulted in limit cycling of the reaction controls and, consequently, required large increases in reaction control system fuel. The system modifications examined were

1. Replacement of the step changes in commanded angle of attack and roll attitudes with linear variations (ramp-like)

2. Modification of a gain in the yaw reaction control system circuit to reduce the roll-rate response to small roll-attitude corrections

3. Modification of a gain to reduce the commanded aileron increment produced by the up-down counter circuit

4. Addition of a hysteresis-deadband filter to the roll-angle error-signal circuit

A combination of the first three modifications resulted in a 64-percent reaction control system fuel savings over the nominal with a 2.00-second sampling time. The combination eliminated system sensitivity to guidance system sampling frequency and limit cycling tendencies. In addition, the combination was relatively insensitive to lateral center-of-gravity offsets and required only a 4-percent increase in reaction control system fuel consumption for the maximum expected offset of 0.038 m (1.5 in.).

Langley Research Center
National Aeronautics and Space Administration
Hampton, VA 23665
June 29, 1976

APPENDIX A

ANALYTIC DRAG CONTROL ENTRY GUIDANCE SYSTEM

The baseline guidance scheme controls the entry by roll modulation while the space shuttle orbiter is flying a preselected angle-of-attack profile. Downrange is controlled by the magnitude of the roll angle, and crossrange is controlled by multiple bank reversals. The guidance system output to the control system is commanded roll angle and angle of attack.

The analytic drag control entry guidance system (ADC) was developed by the NASA Johnson Space Center to approximate an optimum entry profile determined previously. This profile is achieved by dividing the entry into five major phases as illustrated in figure 13:

    (1) Constant attitude phase

    (2) Constant heat-rate phase

    (3) Equilibrium-glide phase

    (4) Constant drag phase

    (5) Transition phase

The space shuttle orbiter is commanded to fly a constant attitude trajectory until a specified total acceleration is attained. At this point, a constant stagnation heat-rate trajectory is flown through pullout to a relative velocity of 6248.4 m/sec (20 500 fps) or until the reference drag level becomes larger than that required to reach the target. If the latter condition is reached, the guidance scheme jumps to the constant drag phase. If this condition is not met, an equilibrium-glide profile is flown either until the reference drag level intersects the constant drag profile required to reach the target and jump to the constant drag phase or until the velocity drops off to 2743.2 m/sec (9000 fps). Whenever the velocity drops to 2743.2 m/sec (9000 fps), the transition phase is entered. During the transition phase, the commanded angle of attack is decreased to the value required at the terminal area energy management (TAEM) point, which occurs at a velocity of

457.2 m/sec (1500 fps) and at an altitude of approximately 21.3 km (70 000 ft).

Table IV shows the input constants that were used, and figure 14 shows the block diagram of the guidance laws.

SYMBOLS

AK dD/dV for constant heat-rate phase, used to define C23, sec^{-1}

ALDREF $(L/D)_{ref}$, used in controller

ALFM   reference equilibrium-glide drag, m/sec^2 (ft/sec^2)

ALMN1   minimum roll command outside of lateral deadband (YB), rad

ALMN2   minimum roll command inside of lateral deadband (YB), rad

ALPCMD   angle-of-attack command, α_c, deg

AMAX1   maximum value function

ARC   distance from intersection with alinement circle to target, m (ft)

ARG $(L/D)_v/(L/D)$, used in roll-command equations, rad

ATK   radius of Earth, m (ft)

BA   equilibrium-glide roll angle used in iteration loop, rad

BAD   final equilibrium-glide roll angle, deg

13

BA1   first iteration equilibrium-glide roll angle, deg

BA2   second iteration equilibrium-glide roll angle, deg

CAGI   temporary calculation used in transition phase to calculate ALDREF and RDTREF, sec^2/m^2 (sec^2/ft^2)

CIGAR   transformation matrix from Earth-centered inertial (ECI) axes to geocentric axes

COSBADD temporary calculation in equilibrium-glide ranging phase used to calculate DREFP

CTH   great circle range from orbiter to target, rad

C4   coefficient used to calculate RDTREF, m/sec (ft/sec)

C5   coefficient used to calculate RDTREF

C11   parameter used to calculate RER1 and RDTREF, m^{-1} (ft^{-1})

C16   coefficient used to calculate LOD1, sec^2/m (sec^2/ft)

C17   coefficient used to calculate LOD1, sec/m (sec/ft)

C21   parameter used to calculate DREFP, RDTREF, SQ, and TT11, m/sec^2 (ft/sec^2)

C22   parameter used to calculate DREFP, E1, E2, RDTREF, SQ, TT11, and TT22, sec^{-1}

C23   parameter used to calculate C22, DREFP, E1, E2, SQ, TT11, and TT22, m^{-1} (ft^{-1})

D   total drag force, N (lb)

DBAR   distance from runway to alinement circle, m (ft)

DBB   increment in roll angle in equilibrium-glide phase, deg

DELAZ   azimuth error, rad

DF   final drag level in transition phase, m/sec^2 (ft/sec^2)

DLIM   control system limit drag level in transition phase, m/sec^2 (ft/sec^2)

DRAG   current drag acceleration level, m/sec^2 (ft/sec^2)

DREFP   drag reference used in controller, m/sec^2 (ft/sec^2)

DT   planar range to target, m (ft)

DTH   angle between alinement circle center and tangency point, rad

DTR $= \pi/180$, rad/deg

DVHEAD   azimuth between runway and heading to tangency point of alinement circle, rad

D23   parameter used to calculate AK, m/sec^2 (ft/sec^2)

EEF   current energy level, m^2/sec^2 (ft^2/sec^2)

EEF4   reference energy level used in transition phase, m^2/sec^2 (ft^2/sec^2)

E1,E2   parameters used to calculate TT22

APPENDIX A

GAMMA   flight-path angle, rad

GCLAT   orbiter geocentric latitude, rad

GCLATT   target geocentric latitude, rad

GS   acceleration of gravity at sea level, m/sec^2 (ft/sec^2)

GSTART   acceleration required to initiate constant heat-rate phase, g units

HA   current altitude, m (ft)

HADOT $= d(HA)/dt$, m/sec (ft/sec)

HDSER   parameter in oblate Earth correction term to RDTREF, m^3/sec (ft^3/sec)

HS   altitude scale height, m (ft)

IDFG2   switching flag in constant drag phase

IDFG3   switching flag in transition phase

IFT   initialization flag in equilibrium-glide phase

ISLECT   phase selector

ISTART   initialization flag

ISTP   iteration flag in equilibrium-glide phase

ISTRT   flag indicating acceleration level equal to GSTART has been reached

ITR   iteration flag in transition phase

L/D   lift-to-drag ratio

$(L/D)_V$ lift-to-drag ratio in vertical plane

LMN   minimum value of LOD1

LN   natural logarithm function

LOD1   desired $(L/D)_V$

PSIE   current heading of orbiter, rad

PSIET   current heading to target, rad

RAZ   runway azimuth, rad

RCG   predicted range in constant drag phase, m (ft)

RDC   parameter used in RDTREF calculation

RDTOLD   final RDTREF in equilibrium-glide phase, m/sec (ft/sec)

RDTOL2   final RDTREF in constant drag phase, m/sec (ft/sec)

RDTREF   altitude rate reference, m/sec (ft/sec)

REC   vector defining runway coordinate system

REC1 $= [REC]^{-1}$

REH   distance from center of Earth to vehicle, m (ft)

REQ   predicted equilibrium-glide phase range, m (ft)

RER1   parameter in range prediction for transition phase, m (ft)

RFF   predicted range in constant heat-rate phase, m (ft)

RG   vector from orbiter to runway center, m (ft)

RGP   vector from orbiter to alinement circle center, m (ft)

RK2ROL   roll direction (+ right, - left)

RLON   longitude of orbiter, rad

RLONT   target longitude, rad

ROLLC   roll-angle command, ϕ_c, rad

RPT   desired range in transition phase, m (ft)

RPT1   range bias below velocity of 456.2 m/sec (1500 fps),
            m (ft)

RTE   radius of Earth at runway, m (ft)

RTURN   radius of alinement circle, m (ft)

R11   first iteration of range prediction in equilibrium-
            glide and transition phases, m (ft)

R12   second iteration of range prediction in equilibrium-
            glide and transition phases, m (ft)

SIGN(A,B)   function which gives to the value of A the
               algebraic sign of the variable B

SQ   parameter used in constant heat-rate range prediction,
            sec^{-2}

SQQ   parameter used in constant heat-rate range prediction,
            sec^{-1}

TA   vector from alinement circle tangency point to
            vehicle, m (ft)

TAP   vector TA in geocentric coordinates, m (ft)

TARE   target vector from alinement circle center to
            runway, m (ft)

TDREF   parameter used in DREFP calculation in equilibrium-
            glide phase, m/sec^2 (ft/sec^2)

TEMP   temporary calculation in equilibrium-glide phase,
            m (ft)

TRANGE   great circle range from orbiter to target, m (ft)

T1   parameter used in calculation of ALDREF, m/sec^2 (ft/sec^2)

T2   constant drag level required to reach target,
            m/sec^2 (ft/sec^2)

TT11,TT22   parameters used in range prediction in constant
            heat-rate phase, m (ft)

U $= |DVHEAD|$, rad

UTARE   TARE unit vector

UXYZE   RG unit vector

APPENDIX A

V   Earth relative velocity, m/sec (ft/sec)

VBB   intersection velocity between constant heat-rate phase
and equilibrium-glide phase, m/sec (ft/sec)

VCG   predicted intersection velocity between constant drag
phase and equilibrium-glide phase, m/sec (ft/sec)

VINERT   inertial velocity, m/sec (ft/sec)

VOLD   final velocity in equilibrium-glide phase, m/sec (ft/sec)

VOLD2   final velocity in constant drag phase, m/sec (ft/sec)

VQ   predicted final velocity for constant drag phase,
m/sec (ft/sec)

VSAT   reference circular orbit velocity, m/sec (ft/sec)

V1OLD   value of VOLD - 152.4 m/sec (500 ft/sec), m/sec (ft/sec)

V2OLD   value of VOLD2 - 152.4 m/sec (500 ft/sec), m/sec (ft/sec)

XLFAC   total acceleration, m/sec^2 (ft/sec^2)

XLOD   L/D of vehicle with undeflected control surfaces
including viscous effects

XYZE   geocentric position vector, m (ft)

YB   lateral deadband (amount of overshoot that guidance
system will allow before commanding roll reversal),
rad

APPENDIX B

DIGITAL AUTOPILOT

Symbols

The following symbols are used in this appendix:

a_Y side acceleration at center of gravity, m/sec^2 (ft/sec^2)

c_e elevon reference chord, m (ft)

c_r rudder reference chord, m (ft)

C_{he} elevon hinge-moment coefficient

C_{h_β} = ∂ (Rudder hinge-moment coefficient)$/\partial\beta$, deg^{-1}

$C_{h_{\delta_r}}$ = ∂ (Rudder hinge-moment coefficient)$/\partial\delta_r$, deg^{-1}

C_{LN} rolling-moment coefficient due to yaw RCS

C_{ML} pitching-moment coefficient due to roll RCS

C_{MN} pitching-moment coefficient due to yaw RCS

C_{NL} yawing-moment coefficient due to roll RCS

DEMX   maximum elevon rate, deg/sec

DRMX   maximum rudder rate, deg/sec

E_P pitch RCS error signal

E_R roll RCS error signal

E_Y yaw RCS error signal

$f(\delta_e)$ function of δ_e used to limit $\delta_{a,c}$, deg

g acceleration of gravity, m/sec^2 (ft/sec^2)

h integration step size, sec

Hm_e elevon hinge moment, N-m (lb-ft)

Hm_r rudder hinge moment, N-m (lb-ft)

K_L rolling-moment RCS amplification factor

K_{MD} pitching-moment RCS amplification factor from down-firing jets

K_{MU} pitching-moment RCS amplification factor from up-firing jets

K_N yawing-moment RCS amplification factor

K_P aileron gain

K_α elevator gain

K_{δ_r} rudder gain

L_{RCS} rolling moment due to RCS, N-m (lb-ft)

L_{RJ} ideal rolling moment due to firing of one roll jet, N-m (lb-ft)

M Mach number

M_{PJ} ideal pitching moment due to firing of one pitch jet, N-m (lb-ft)

M_{RCS} pitching moment due to RCS, N-m (lb-ft)

N_{RCS} yawing moment due to RCS, N-m (lb-ft)

N_{YJ} ideal yawing moment due to firing of one yaw jet, N-m (lb-ft)

p roll rate, deg/sec

P convolution coefficient

PJN number of negative pitch jets firing

PJP number of positive pitch jets firing

q pitch rate, deg/sec

$\bar{q}$ dynamic pressure, Pa (psf)

q_1 convolution coefficient, sec

q_2 convolution coefficient, sec^2

$\bar{Q}$ vector of convolution coefficients

r yaw rate, deg/sec

r' $= r - (180g \sin \phi \cos \theta)/\pi V_R$, deg/sec

RJN number of negative roll jets firing

RJP number of positive roll jets firing

s   Laplacian operator

S_e elevon reference area, m^2 (ft^2)

S_r rudder reference area, m^2 (ft^2)

t   time, sec

t_k time at kth sample, sec

U   convolution forcing function

$\bar{U}$ vector of forcing-function terms

$\dot{U}$ $= dU/dt$

V_R Earth relative velocity, m/sec (ft/sec)

W   filter root, sec^{-1}

x   convolution state variable

$\dot{x}$ $= dx/dt$

YJN   number of negative yaw jets firing, nondimensional

YJP   number of positive yaw jets firing, nondimensional

α angle of attack, deg

α_c commanded angle of attack from guidance system, deg

β angle of sideslip, deg

δ_a aileron deflection, deg

24

$\delta_{a,c}$ commanded aileron deflection, deg

$\delta_{a,UD}$ commanded aileron deflection from up-down counter, deg

δ_{BF} body-flap deflection, deg

δ_e elevator deflection, deg

$\delta_{e,c}$ commanded elevator deflection, deg

$\delta_{e\ell}$ left elevon panel deflection, deg

$\delta_{e\ell,c}$ command left elevon panel deflection, deg

$\delta_{e,\ell m}$ maximum change in elevon command that can be realized in one control cycle, deg

δ_{er} right elevon panel deflection, deg

$\delta_{er,c}$ commanded right elevon panel deflection, deg

$\delta_{e,t}$ initial elevator setting, deg

δ_r rudder deflection, deg

$\delta_{r,c}$ commanded rudder deflection, deg

$\delta_{r,\ell m}$ maximum change in rudder command that can be realized in one control cycle, deg

δ_{SB} speed-brake deflection, deg

θ pitch angle, deg

ϕ roll angle, deg

ϕ_c commanded roll angle to control system, deg

τ variable of integration, sec

Description of Digital Autopilot

The digital autopilot (DAP) is designed to fly the space shuttle orbiter automatically from deorbit to the terminal area energy management (TAEM) interface which occurs at an altitude of approximately 21.3 km (70 000 ft) with a velocity of 457.2 m/sec (1500 fps). The DAP directs both the reaction control system (RCS) and the aerodynamic control surfaces.

The speed-brake δ_{SB} and body-flap δ_{BF} deflection schedules are shown in figure 15, where δ_{SB} is determined from a preset velocity schedule and δ_{BF} is dependent on the center-of-gravity location. Figures 16 to 24 are block diagrams of the various elements of the DAP. Two types of signal limiting filters are used in this autopilot. The first type is illustrated in sketch (c):
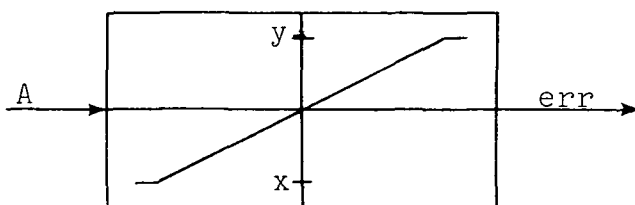
Sketch (c)

This filter limits the value of the quantity A to be between x and y. The second type, called a hysteresis filter, can appear in one of two ways (sketch (d)):

(1)   (2)

Sketch (d)
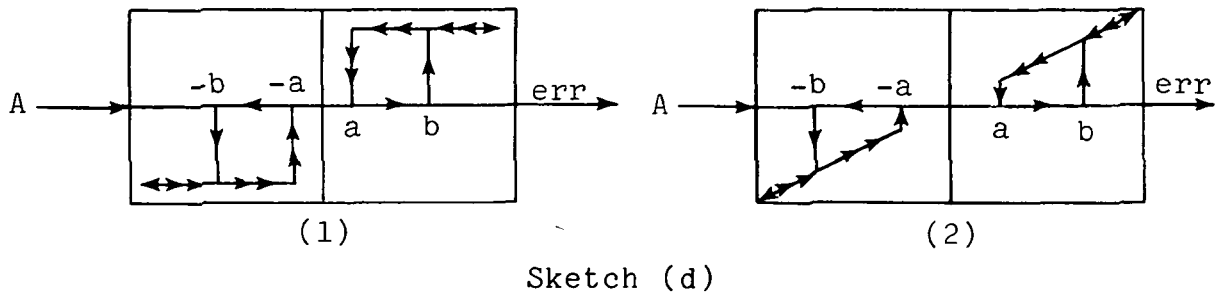
As A increases from zero, err remains zero until point b is
reached. At this time, err becomes the value indicated (either
a constant value if filter is type 1 or equal to A if filter is
type 2). As A starts to decrease, it remains the value indicated
until point a is reached where err becomes zero again. A simi-
lar situation would exist for an A decreasing from zero.

The elevons are used for both elevator δ_e and aileron δ_a
functions. The elevator command block diagram is shown in fig-
ure 16. The aileron functions in one of two ways depending on
the flight regime: for $\alpha \leq 18°$ and $M \leq 5$, the aileron is used
for roll-attitude ϕ control (fig. 17(a)); when these conditions
are not present, the ailerons are used for turn coordination
(fig. 17(b)).

If the orbiter has a lateral center-of-gravity offset, the
number of positive yaw and roll thruster firings are not equal to
the number of negative yaw and roll thruster firings caused by the
induced sideslip. By counting the number of positive and negative
yaw and roll thruster firings, it is possible to establish the
steady-state aileron deflection required to offset this induced
sideslip. The establishment of this aileron deflection is the
role of the up-down counter shown in figure 18. The numbers in
parentheses in the block diagrams are the expressed values in U.S.
Customary Units.

Figure 19 shows that the commanded left and right elevon
deflections are functions of δ_e, $\delta_{a,c}$, and $\delta_{e,c}$. The rudder δ_r
(fig. 20) is used for turn coordination when the aileron is used
for roll control. If the ailerons are being used for turn coordi-
nation, the rudder is inoperative.

The pitch RCS (fig. 21) is operative for $\bar{q}$ less than 958 Pa (20 psf). In this regime the pitch RCS is used, along with the elevator, for longitudinal control.

The roll RCS (fig. 22) is operative for $\bar{q}$ less than 479 Pa (10 psf) and is used, together with the ailerons, for turn coordination.

The yaw RCS (fig. 23) is operative throughout the entry until TAEM and serves one of two purposes depending on the flight conditions. If the ailerons are used for attitude control, the yaw RCS (fig. 23(a)) aids the rudder in maintaining turn coordination. If the conditions are such that the ailerons are used for turn coordination, the yaw RCS (fig. 23(b)) is used for roll-attitude ϕ control.

To integrate the linear first-order differential equations in the control system, the convolution technique is used. This technique is a one-pass scheme that has demonstrated a high degree of accuracy in other real-time simulations, including piloted simulations. A typical first-order system

$$\dot{x}(t) + W\, x(t) = U(t)$$

where $U(t)$ is the forcing function, is illustrated in sketch (e):

$$U(s) \rightarrow \boxed{\frac{1}{s+W}} \rightarrow x(s)$$
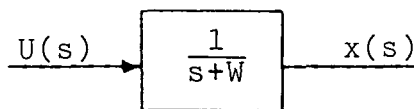
Sketch (e)

The solution is

$$x(t) = e^{-Wt}\, x(0) + \int_0^t e^{-W(t-\tau)}\, U(\tau)\, d\tau$$

The convolution technique is a numerical method based on a Taylor series approximation (first two terms) of the forcing function U and results in the following difference equation:

28

$$x(t_k + h) = P(h) \, x(t_k) + \bar{Q}(h) \, \bar{U}(t_k)$$

where

$$P(h) = e^{-Wh}$$

$$\bar{Q}(h) = \begin{bmatrix} q_1(h), & q_2(h) \end{bmatrix}$$

$$\bar{U}(t_k) = \begin{bmatrix} U(t_k) \\ \dot{U}(t_k) \end{bmatrix}$$

$$q_1(h) = \int_0^h e^{-W(h-\tau)} \, d\tau = \frac{1 - e^{-Wh}}{W} = \frac{1 - P}{W}$$

$$q_2(h) = \int_0^h \tau e^{-W(h-\tau)} \, d\tau = \frac{-1 - e^{-Wh} + Wh}{W^2} = \frac{h - q_1}{W}$$

The control actuators (fig. 24) are integrated the same way, except that provisions are made for both position and rate limits.

The RCS model uses the following equations to account for aerodynamic interference:

$$L_{RCS} = L_{RJ} \left[(RJP - RJN)K_L + (YJP - YJN)C_{LN} \right]$$

$$M_{RCS} = M_{PJ} \left[(PJP)K_{MU} - (PJN)K_{MD} + (YJP + YJN)C_{MN} \right.$$
$$\left. + (RJP + RJN)C_{ML} \right]$$

$$N_{RCS} = N_{YJ} \left[(YJP - YJN)K_N + (RJP - RJN)C_{NL} \right]$$

The values for the coefficients are shown in table V.

REFERENCE

1. Malkin, M. S.: Space Shuttle/The New Baseline. Astronaut. &
   Aeronaut., vol. 12, no. 1, Jan. 1974, pp. 62-68.

TABLE I.- PHYSICAL CHARACTERISTICS OF SPACE SHUTTLE ORBITER

Mass properties:
  Mass, kg (lb) 83 001 (182 986)
  Moments of inertia:
    I_{XX}, kg-m^2 (slug-ft^2) 1 029 066 (759 000)
    I_{YY}, kg-m^2 (slug-ft^2) 7 816 290 (5 765 000)
    I_{ZZ}, kg-m^2 (slug-ft^2) 8 015 596 (5 912 000)
    I_{XZ}, kg-m^2 (slug-ft^2) 177 612 (131 000)
    $I_{XY} = I_{YZ} = 0$
Wing:
  Reference area, m^2 (ft^2) 249.91 (2690.0)
  Chord, m (ft) 12.06 (39.57)
  Span, m (ft) 23.79 (78.06)
Elevon:
  Reference area, m^2 (ft^2) 19.51 (210.0)
  Chord, m (ft) 2.30 (7.56)
Rudder:
  Reference area, m^2 (ft^2) 9.30 (100.15)
  Chord, m (ft) 1.86 (6.1)
Body flap:
  Reference area, m^2 (ft^2) 12.54 (135.0)
  Chord, m (ft) 2.06 (6.75)

TABLE II.- EFFECT OF GUIDANCE SYSTEM SAMPLE TIME ON RCS FUEL CONSUMPTION

[Control system sample time 0.04 second]

Period	RCS fuel consumption, kg (lb), for guidance system sample time, sec, of -						
	0.04	0.08	0.16	0.32	0.64	1.28	2.00
Entire entry	187.0 (412.2)	197.5 (435.5)	187.9 (414.3)	197.0 (434.3)	203.6 (448.8)	304.1 (670.4)	385.6 (850.2)
First 500 seconds	81.6 (180.0)	80.3 (177.0)	80.9 (178.4)	89.1 (196.5)	93.2 (205.5)	160.2 (353.2)	180.3 (397.4)

TABLE III.- EFFECT OF SYSTEM MODIFICATIONS ON
RCS FUEL CONSUMPTION

Modification	RCS fuel consumption for guidance system sample times of -					
	0.32 sec		1.28 sec		2.00 sec	
	kg	lb	kg	lb	kg	lb
Without mods	197.0	434.3	304.1	670.4	385.6	850.2
Ramp	191.4	422.0	187.5	413.4	189.4	417.6
Gain	171.9	379.0	196.0	432.0	236.4	521.3
Up-down gain	176.5	389.1	284.0	626.2	378.2	833.9
Hysteresis for -						
$\quad$ a = 1.5°	198.3	437.2	293.1	646.2	387.8	855.0
$\quad$ b = 3.0°						
$\quad$ a = 3.0°	400.7	883.3	440.6	971.4	452.1	996.7
$\quad$ b = 4.5°						
Ramp + Gain	162.5	358.3	155.4	342.6	160.4	353.8
Ramp + Gain + Up-down gain	139.1	306.6	135.6	299.0	140.3	309.4
Ramp + Gain,	172.5	380.4	173.2	381.9	167.1	368.3
$\quad y_{cg}$ = 0.038 m (1.5 in.)						
Ramp + Gain + Up-down gain,	146.7	323.4	142.7	314.6	146.0	321.9
$\quad y_{cg}$ = 0.038 m (1.5 in.)						

TABLE IV.- ANALYTIC DRAG CONTROL GUIDANCE INPUT CONSTANTS

Parameter	Value	Unit
ALFM	7.62 (25)	m/sec^2 (ft/sec^2)
ALMN1	0.7986355	Nondimensional
ALMN2	0.9659258262	Nondimensional
ATK	6366707.02 (2.08881464×10^7)	m (ft)
DBAR	14 360.4 (48 000)	m (ft)
DF	5.819 (19.09)	m/sec^2 (ft/sec^2)
EEF4	185806.08 (2.0×10^6)	m^2/sec^2 (ft^2/sec^2)
GCLATT	34.55577617	deg
GS	9.815 (32.2)	m/sec^2 (ft/sec^2)
GSTART	0.05	Nondimensional
RAZ	-0.7679448709	rad
RLONT	-120.5338	deg
RPT	421885.6 (1.3841391×10^6)	m (ft)
RPT1	23 150 (75 951.4)	m (ft)
RTE	6373298.953 (2.090977347×10^7)	m (ft)
RTURN	4 632.96 (15 200)	m (ft)
VQ	2 133.6 (7 000)	m/sec (ft/sec)
VSAT	7 853.54 (25 766.2)	m/sec (ft/sec)

TABLE V.- INTERFERENCE RCS VALUES

Jet moment	Value, N-m (lb-ft)
L_{RJ}	11 185.5 (8 250.0)
M_{PJ}	38 325.6 (28 267.5)
N_{YJ}	38 878.8 (28 675.5)

$\bar{q}$, Pa (psf)	K_L	K_{MU}	K_{MD}	K_N	C_{LN}	C_{MN}	C_{ML}	C_{NL}
0	0.746	1.0	0.740	1.02	-0.624	0	0.130	-0.141
119.7 (2.5)	.688	1.0	.678	1.02	-.953	.038	.161	-.115
239.4 (5.0)	.630	1.0	.616	1.02	-1.069	.076	.192	-.111
478.8 (10.0)	.533	1.0	.541	1.02	-1.069	.114	.230	-.111
718.2 (15.0)	.475	1.0	.512	1.02	-1.069	.133	.244	-.111
957.6 (20.0)	.436	1.0	.493	1.02	-1.069	.152	.253	-.111

M	K_N	C_{LN}	C_{MN}
q > 957.6 Pa (20 psf)			
2	1.02	-0.701	0.076
5	1.02	-.934	.076
10	1.02	-1.166	.076
30	1.02	-1.069	.152

Elevon

Elevon

Rudder (flares as
speed brake)

RCS location

Body flap
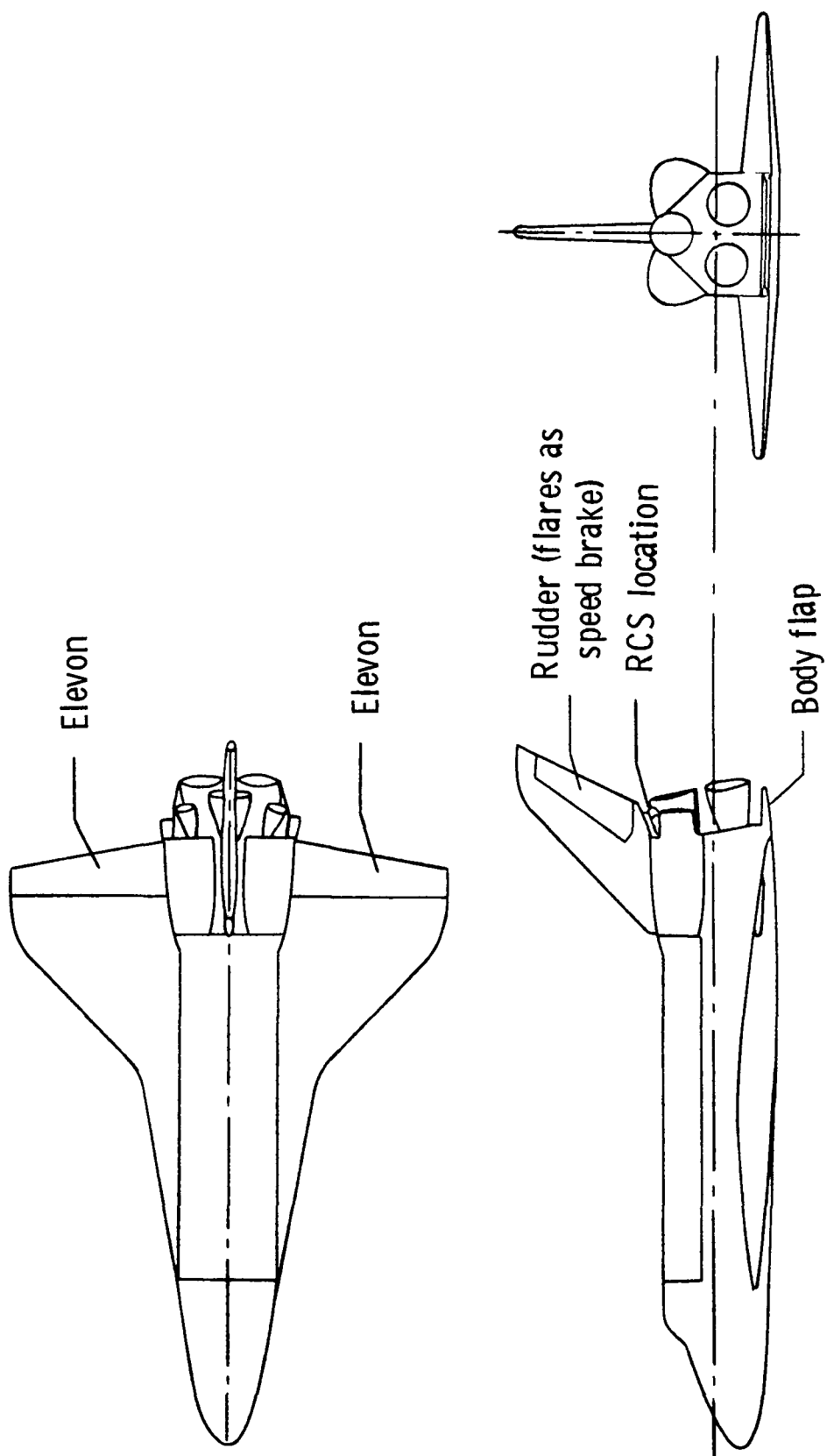
Figure 1.- Space shuttle orbiter.
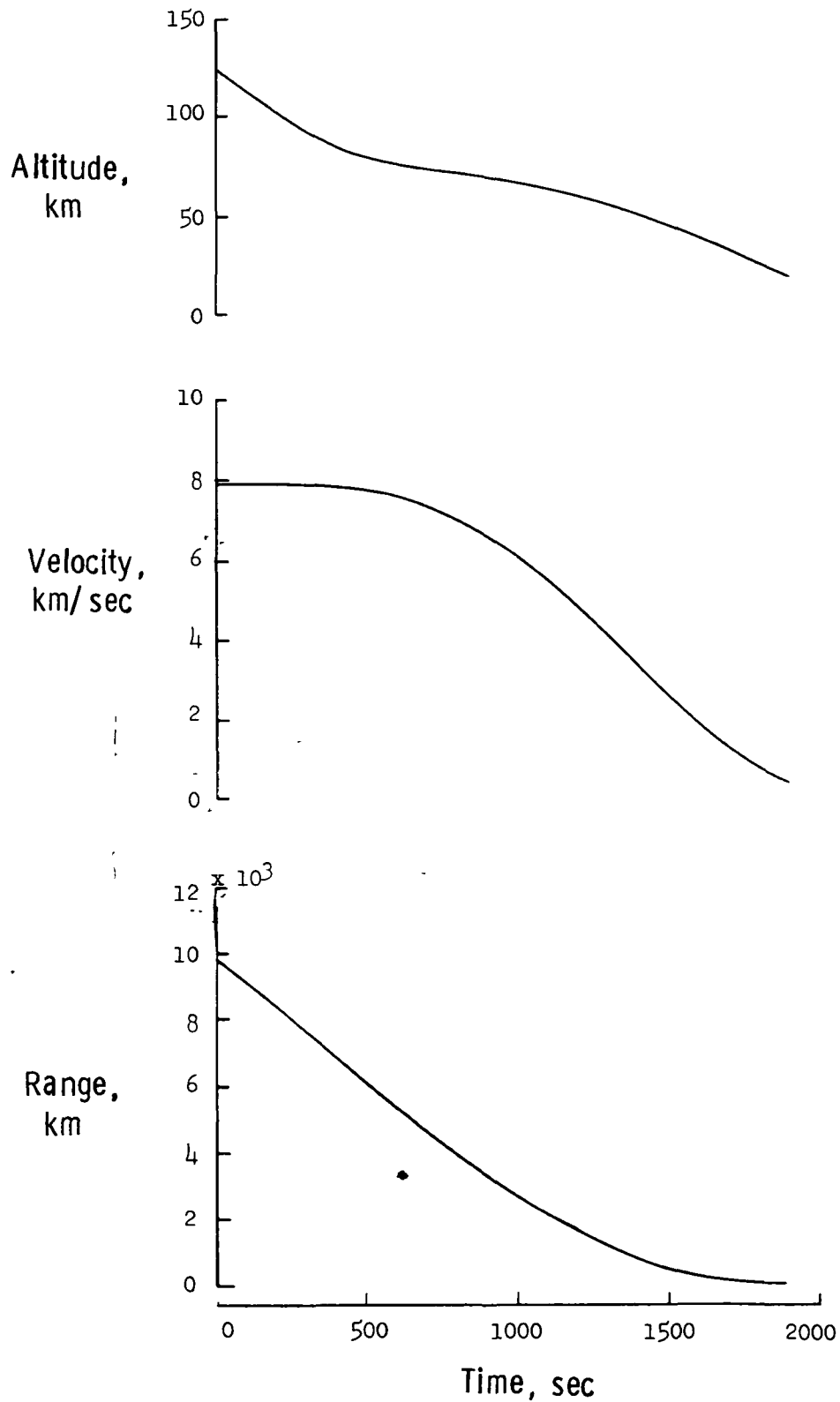
Figure 2.- Space shuttle orbiter entry trajectory parameters.
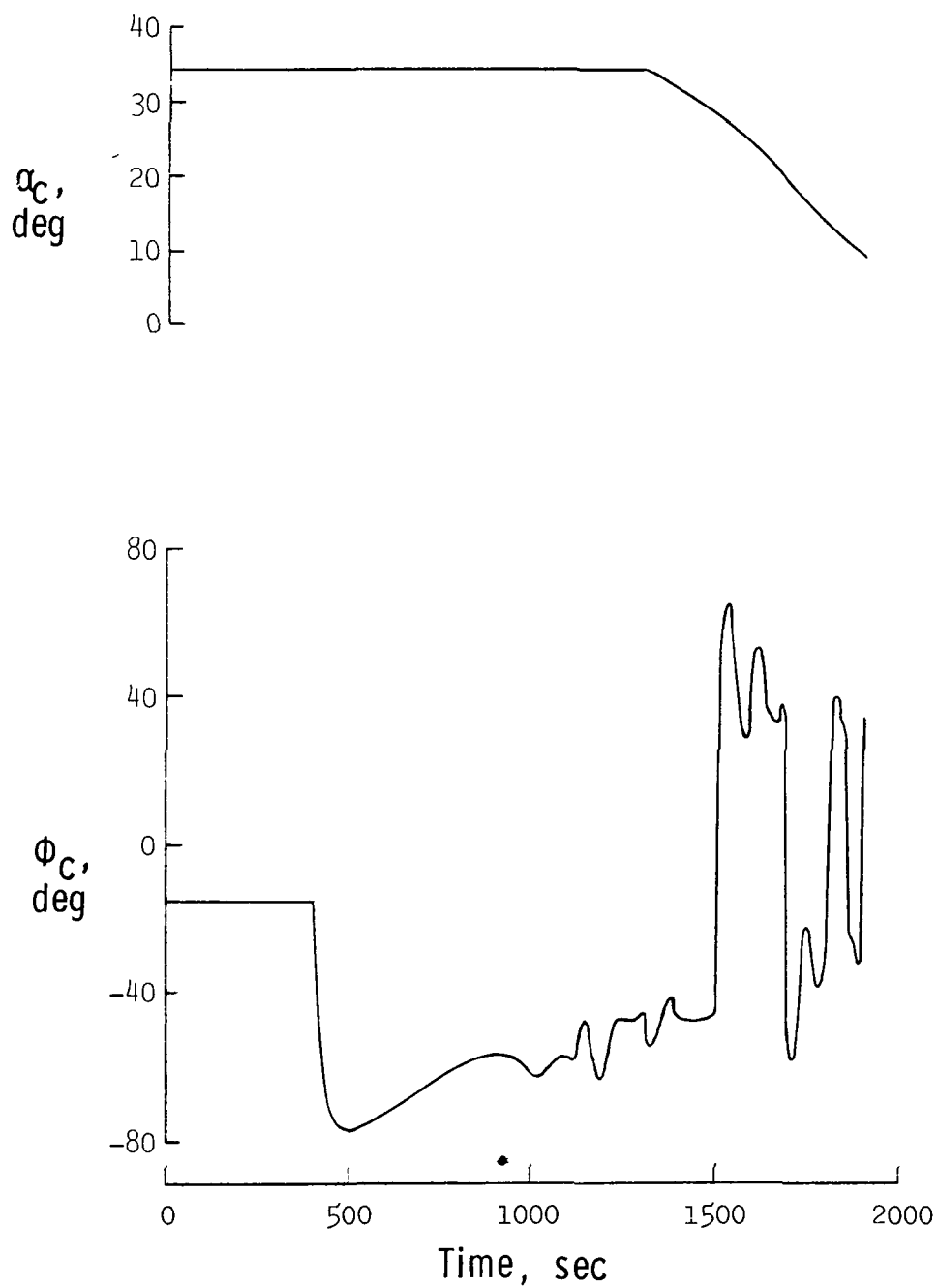
Figure 2.- Concluded.
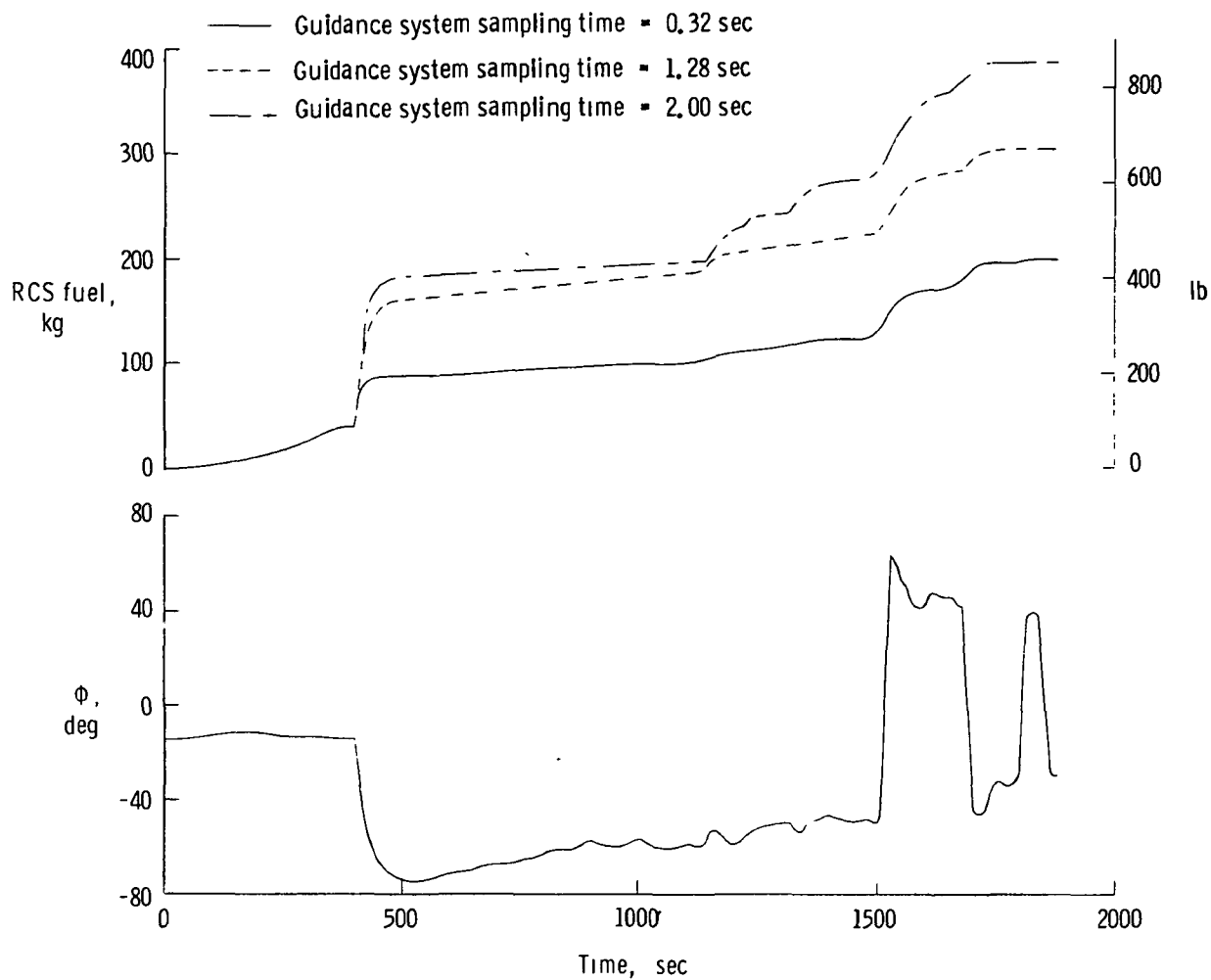
Figure 3.- RCS fuel and roll-angle ϕ histories for various guidance system sampling times.
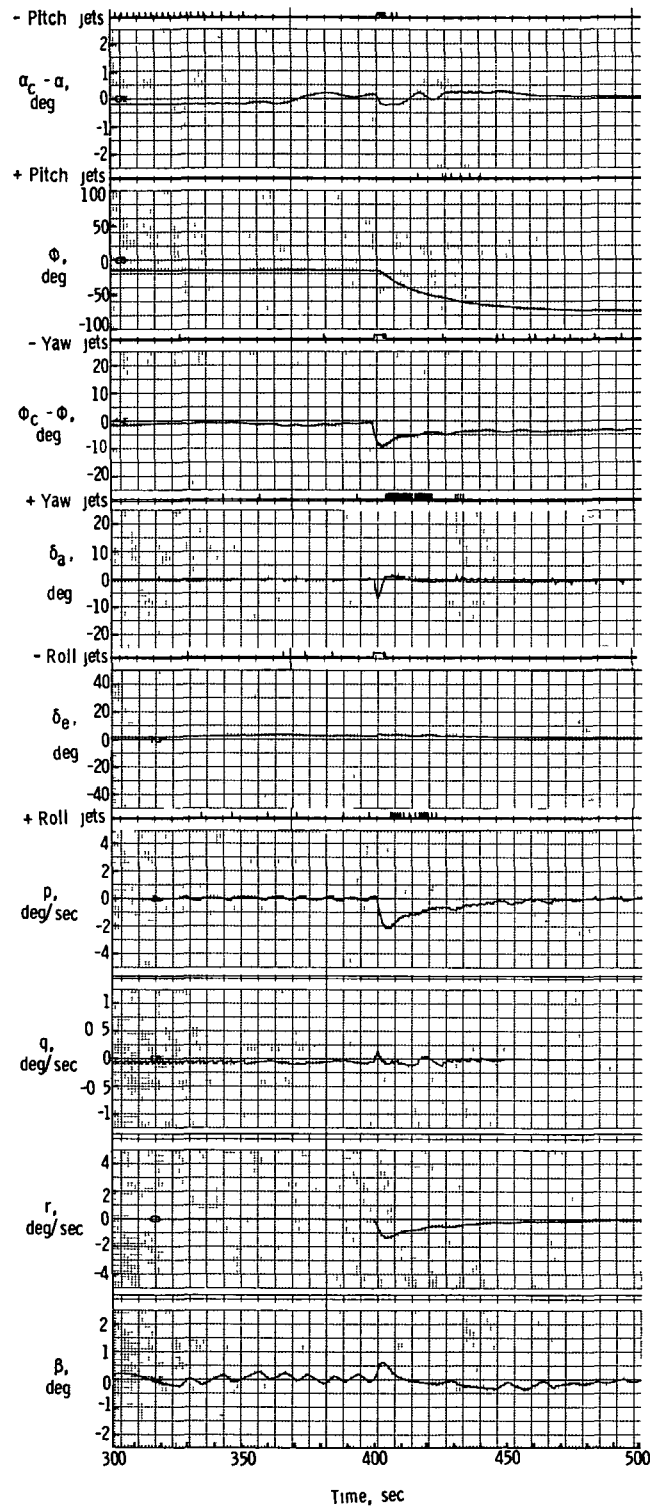
(a) Guidance system sampling time - 0.32 sec.

Figure 4.- Simulation strip charts for various guidance system sampling times.
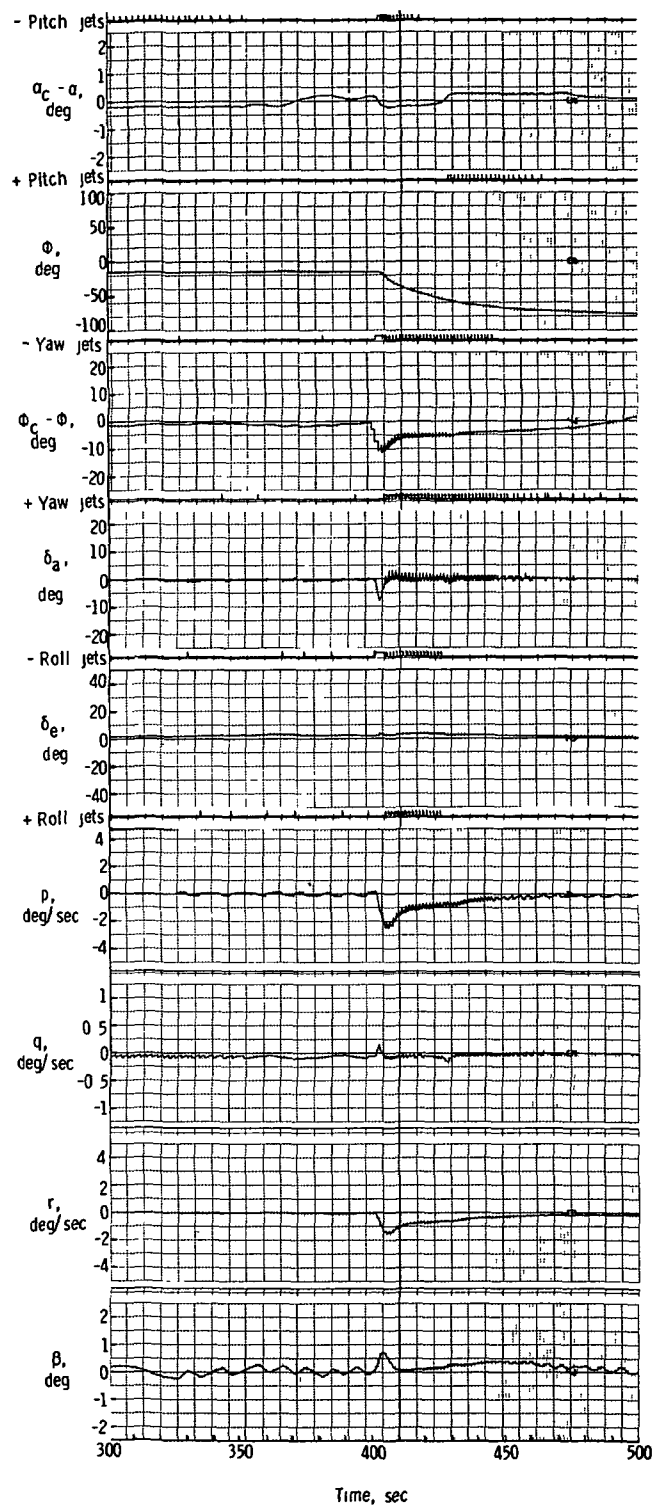
(b) Guidance system sampling time - 1.28 sec.

Figure 4.- Continued.
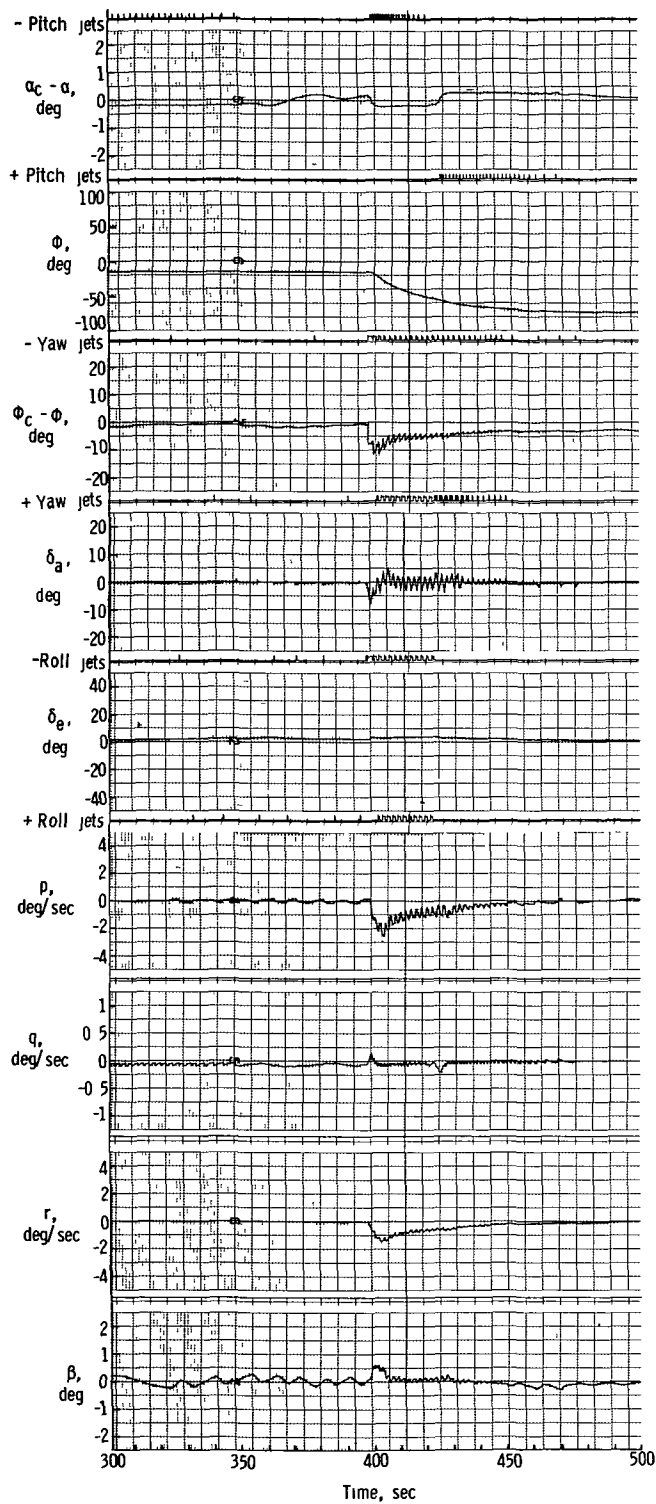
(c) Guidance system sampling time - 2.00 sec.

Figure 4.- Concluded.
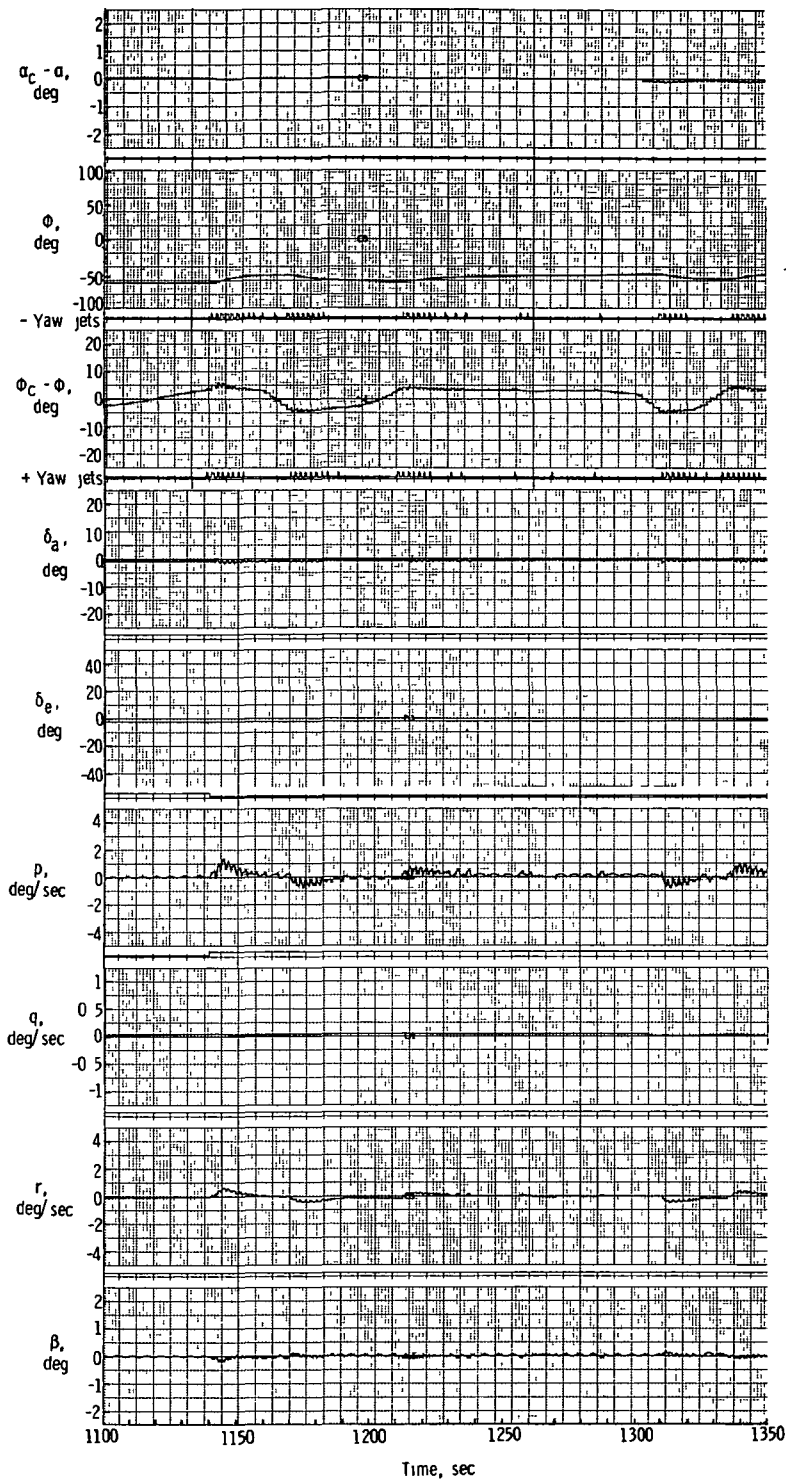
Figure 5.- Simulation strip charts for early portion of constant drag phase with guidance sampling time of 2.00 sec.

Figure 6.- Simulation strip charts for later portion of entry
with guidance sampling time of 2.00 sec.
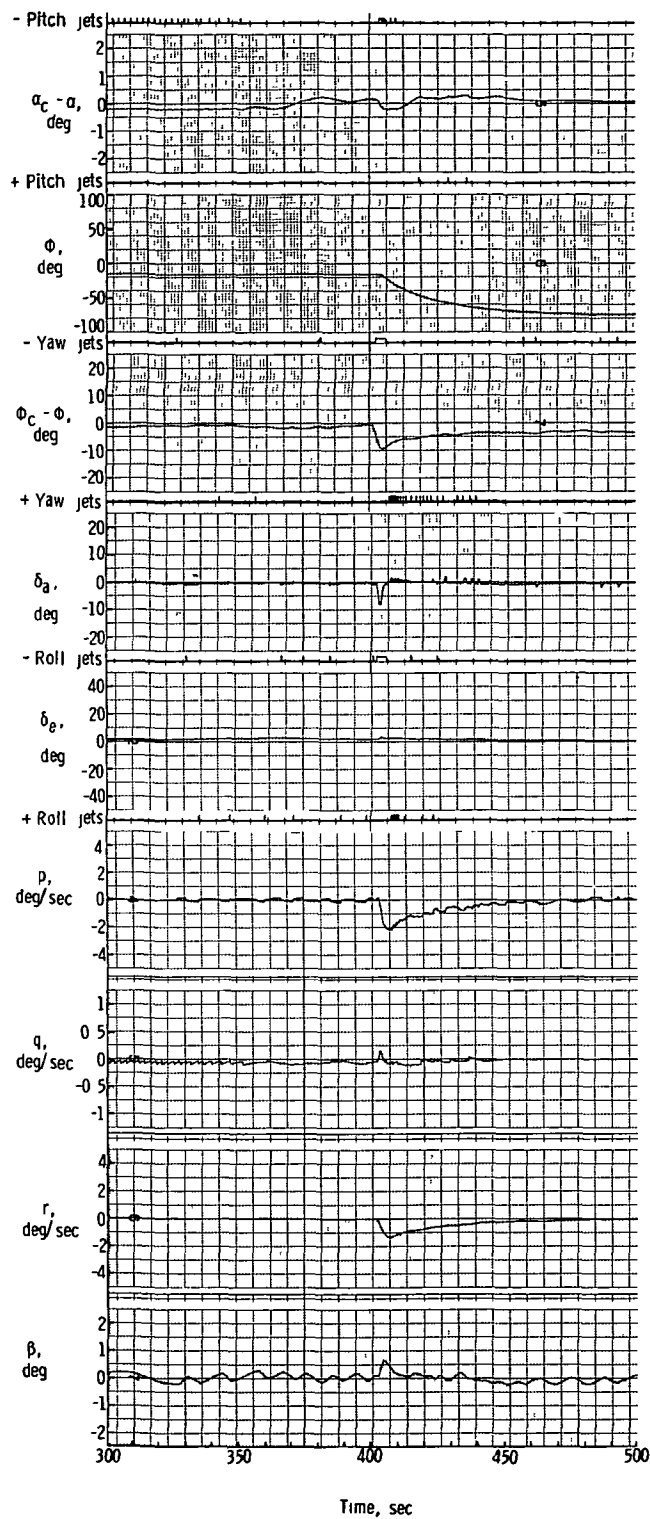
(a) Early portion of entry.

Figure 7.- Simulation strip charts for ramp with guidance
sampling time of 2.00 sec.
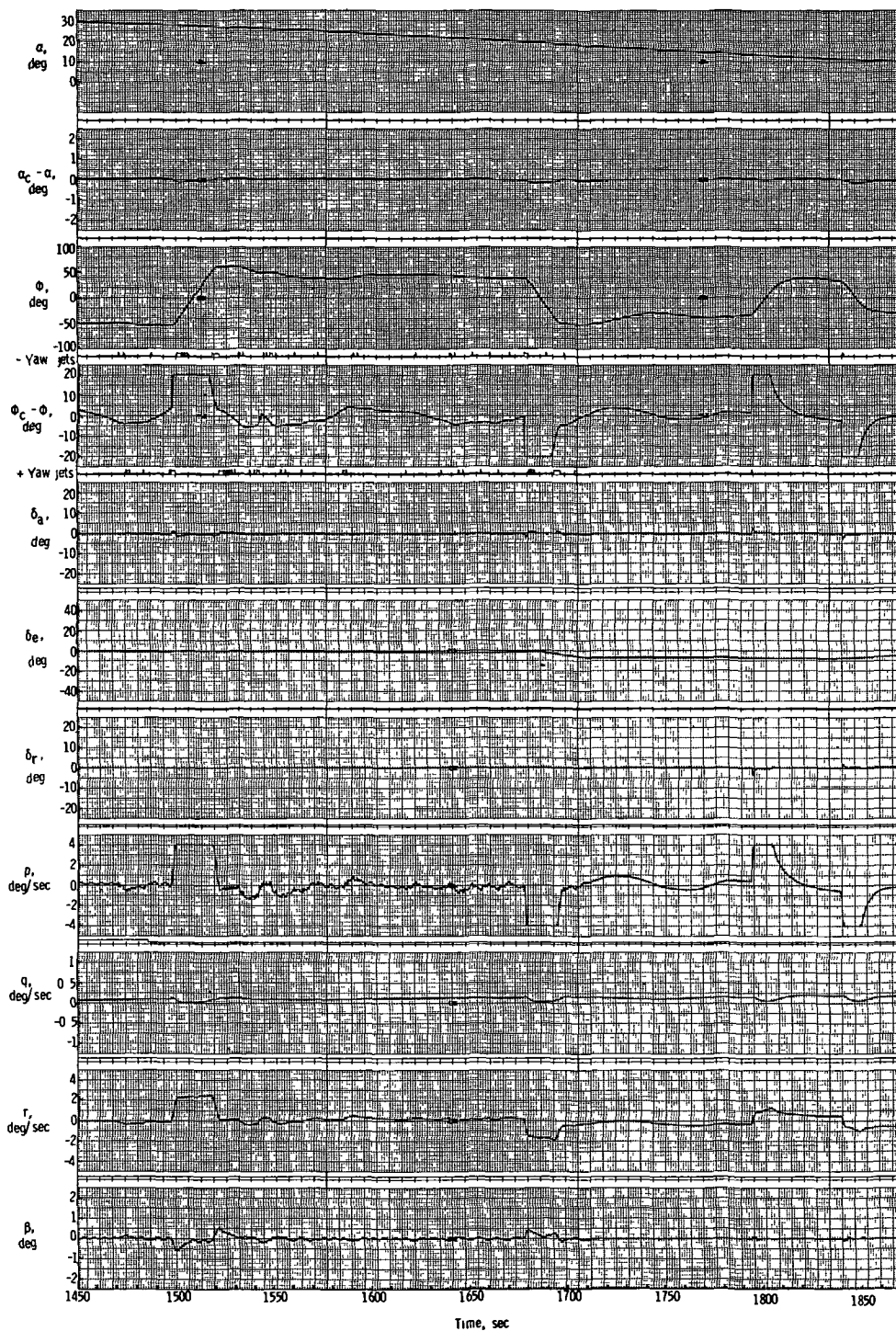
(b) Final portion of entry.

Figure 7.- Concluded.
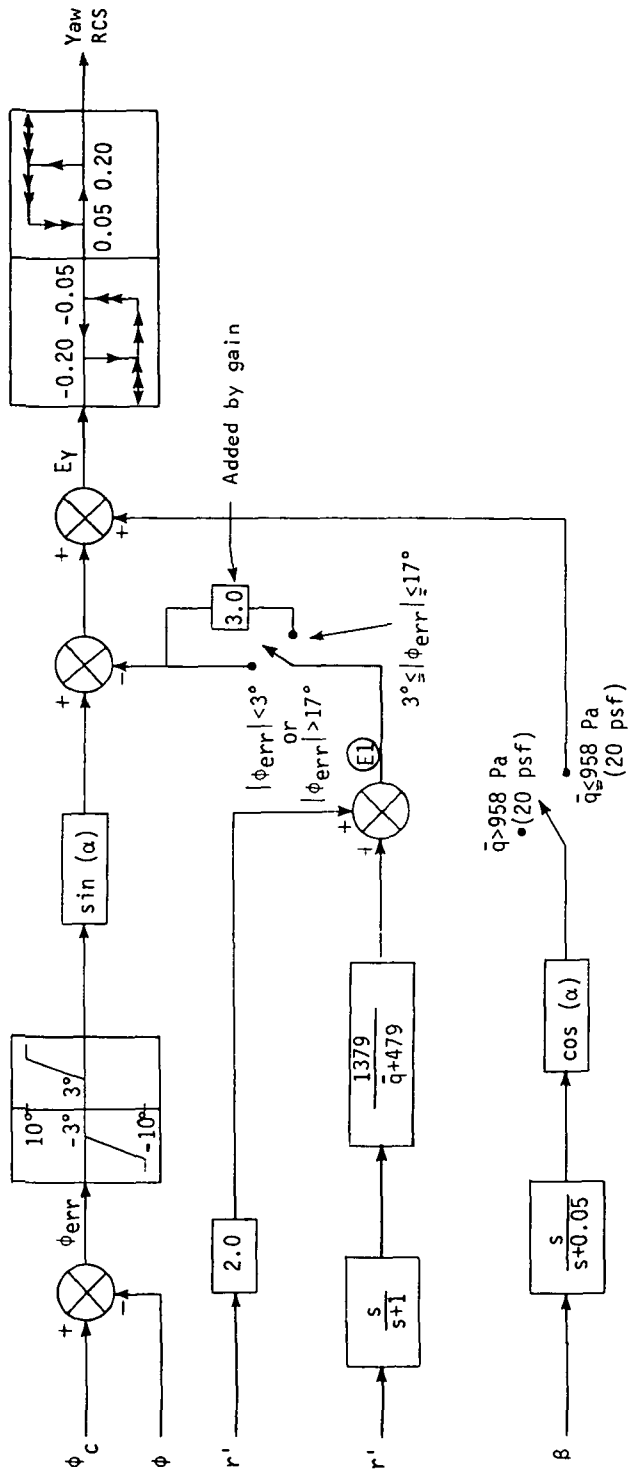
Figure 8.- Yaw RCS block diagram modified by gain.
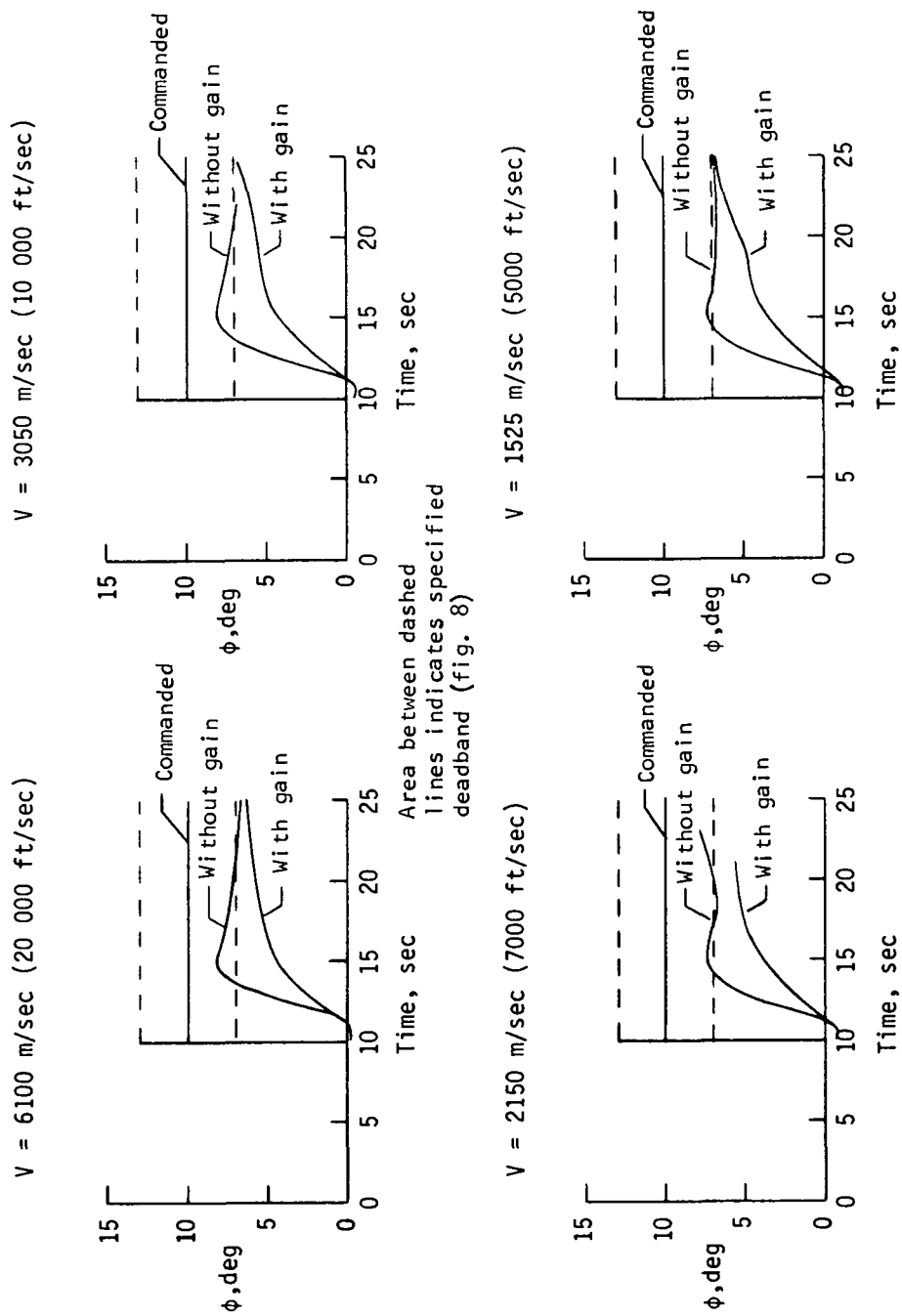
Figure 9.- Effect of gain on roll response.
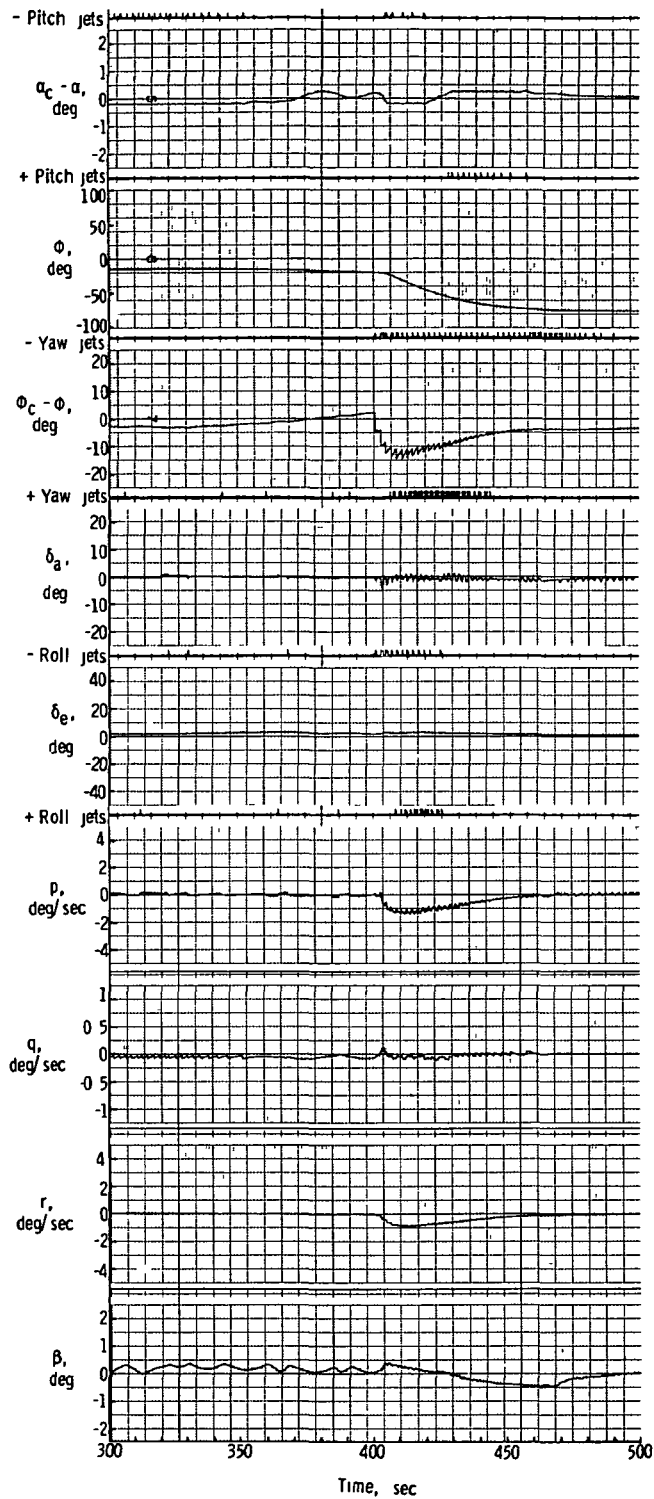
(a) Early portion of entry.

Figure 10.- Simulation strip charts for gain with guidance sampling time of 2.00 sec.
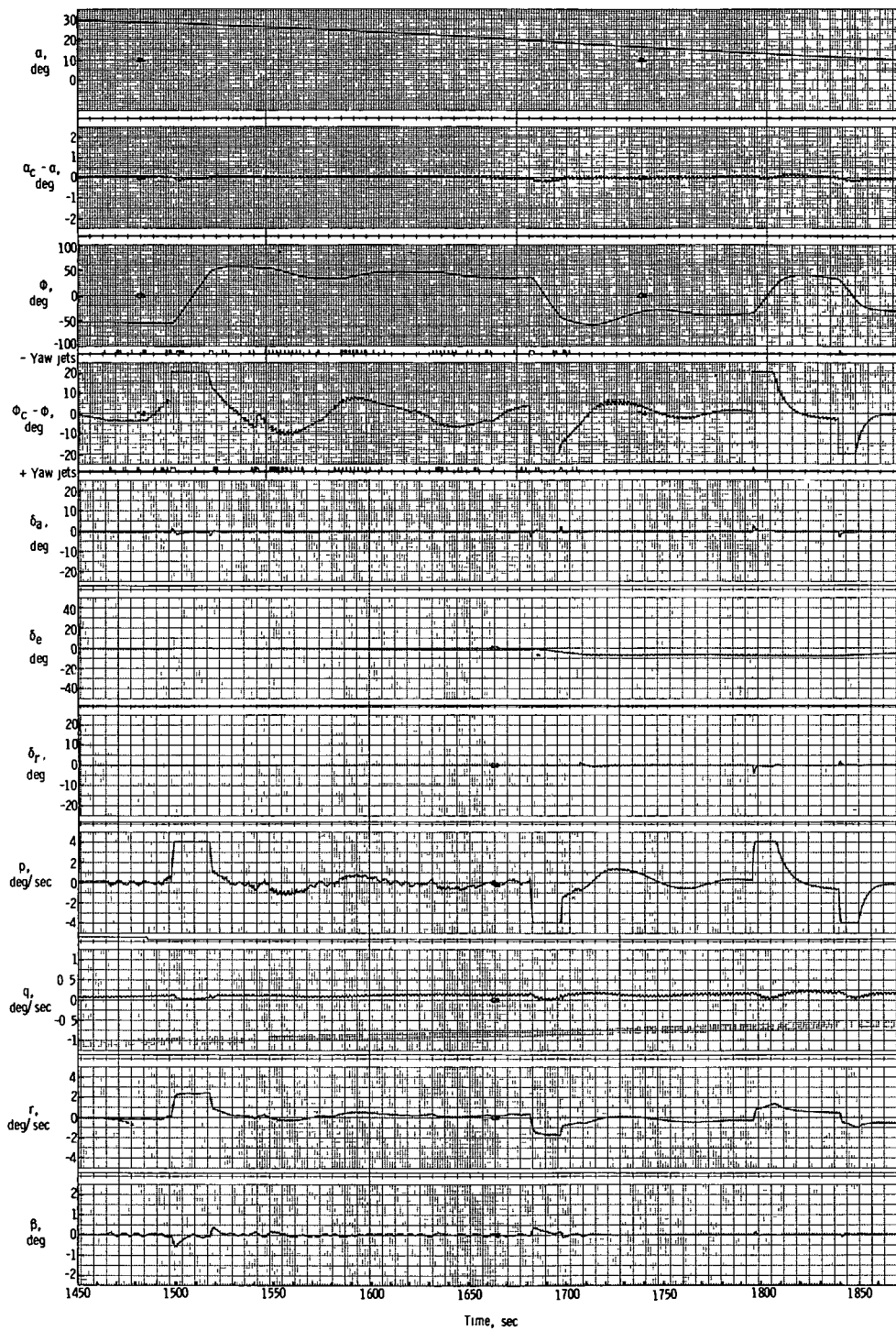
(b) Final portion of entry.

Figure 10.- Concluded.
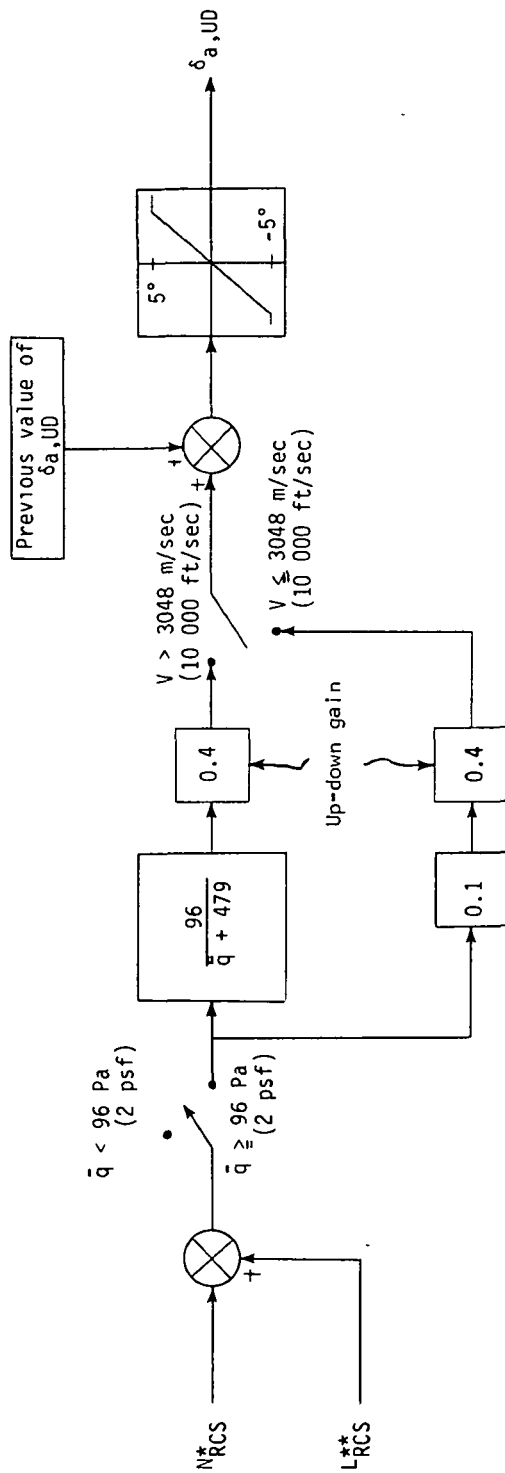
Figure 11.— Up-down counter block diagram modified by up-down gain.

*Number of yaw jets that came on (+ for positive jet, − for negative jet).

**Number of roll jets that came on (+ for positive jet, − for negative jet).

51
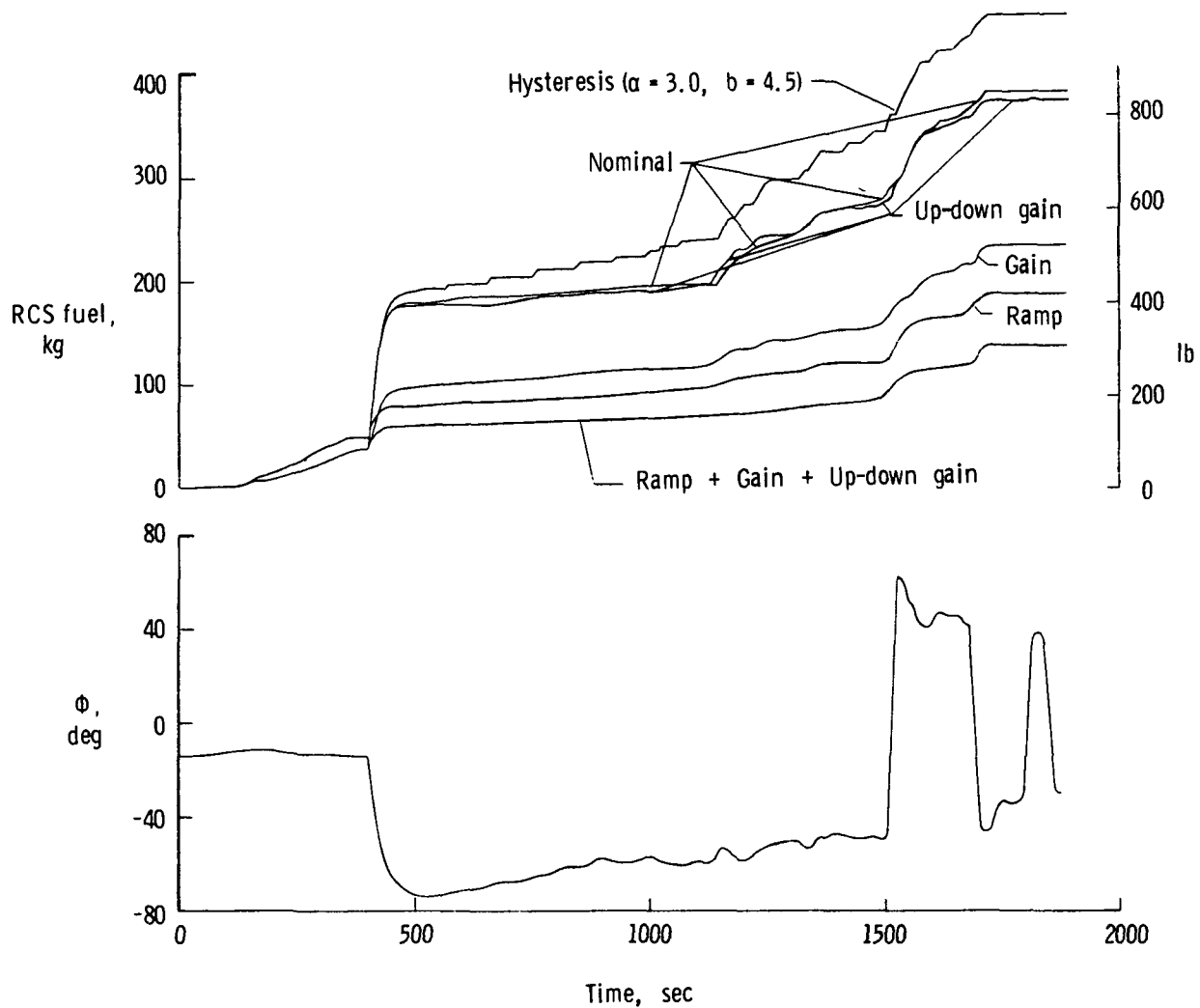
Figure 12.- RCS fuel and roll-angle ϕ histories for various control system modifications with guidance system sampling time of 2.00 sec.
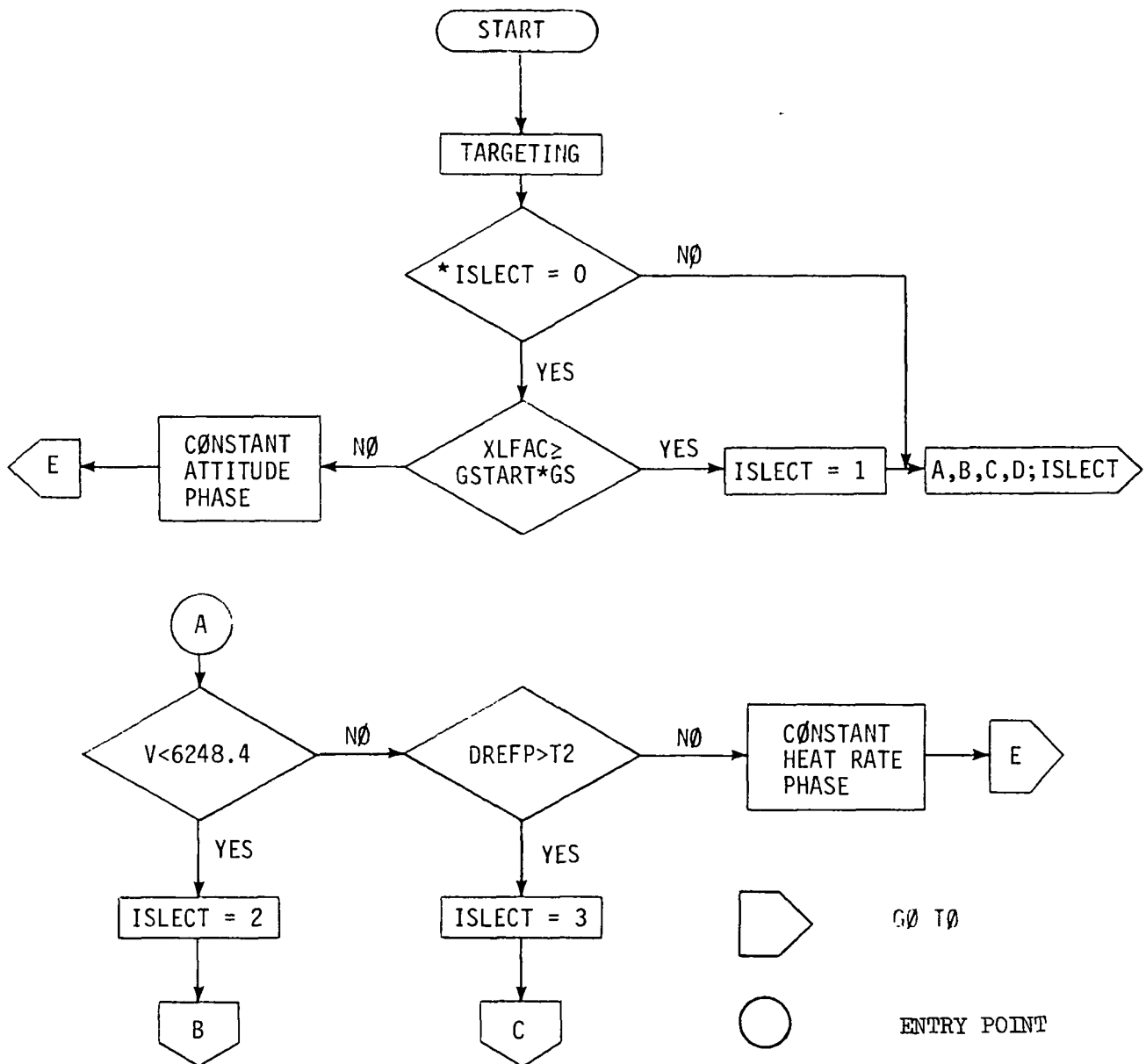
*ISLECT = 0 initially

Figure 13.- Analytic drag control entry guidance system
flow diagram.

Figure 13.- Concluded.

```
                    ┌─────────────┐
                    │ INITIALIZE  │
                    └──────┬──────┘
                           │
                           ▼
        ┌──────────────────────────────────────┐
        │  DATA   GS,ATK,GSTART,RPT,            │
        │         VSAT,VQ,ALMN1,ALFM,           │
        │         RPT1,RAZ,RTE,DBAR,            │
        │         RTURN,ALMN2,EEF4,DF,          │
        │         RLØNT,GCLATT                  │
        └──────────────────┬───────────────────┘
                           │
                           ▼
┌────────────────────────────────────────────────────────────────┐
│ REC(1,1) = -CØS(RAZ)*SIN(GCLATT)*CØS(RLØNT)-SIN(RAZ)*SIN(RLØNT)  │
│ REC(1,2) = -CØS(RAZ)*SIN(GCLATT)*SIN(RLØNT)+SIN(RAZ)*CØS(RLØNT)  │
│ REC(1,3) = CØS(RAZ)*CØS(GCLATT)                                  │
│ REC(2,1) = SIN(RAZ)*SIN(GCLATT)*CØS(RLØNT)-CØS(RAZ)*SIN(RLØNT)   │
│ REC(2,2) = SIN(RAZ)*SIN(GCLATT)*SIN(RLØNT)+CØS(RAZ)*CØS(RLØNT)   │
│ REC(2,3) = -SIN(RAZ)*CØS(GCLATT)                                 │
│ REC(3,1) = -CØS(GCLATT)*CØS(RLØNT)                               │
│ REC(3,2) = -CØS(GCLATT)*SIN(RLØNT)                               │
│ REC(3,3) = -SIN(GCLATT)                                          │
└────────────────────────────────┬───────────────────────────────┘
                                  │
                                  ▼
                    ┌──────────────────────────┐
                    │ ISTRT = 0                │
                    │ ISTART = 0               │
                    │ ISLECT = 0               │
                    │ IFT = 0                  │
                    │ IDFG2 = IDFG3 = 0        │
                    │ ISTP = 0                 │
                    └────────────┬─────────────┘
                                 │
                                 ▼
                    ┌──────────────────────────┐
                    │ BA1 = 0.                 │
                    │ VBB = 6248.4             │
                    │ YB  = .3054              │
                    └────────────┬─────────────┘
                                 │
                                 ▼
                    ┌──────────────────────────┐
                    │   GUIDANCE EQUATIØNS     │
                    └────────────┬─────────────┘
                                 │
                                 ▼
                          ╱──────────╲
                         ╱    TIME    ╲        NØ      ┌────────┐
                        ◄   TØ SAMPLE  ►──────────────▶│  DD   ╱
                         ╲  GUIDANCE? ╱                └────────┘
                          ╲──────────╱
                                 │
                                YES
                                 │
                                 ▼
                              ┌─────╲
                              │  A  │
                              └─────╱
```

Figure 14.- Analytic drag control entry guidance system
block diagram.
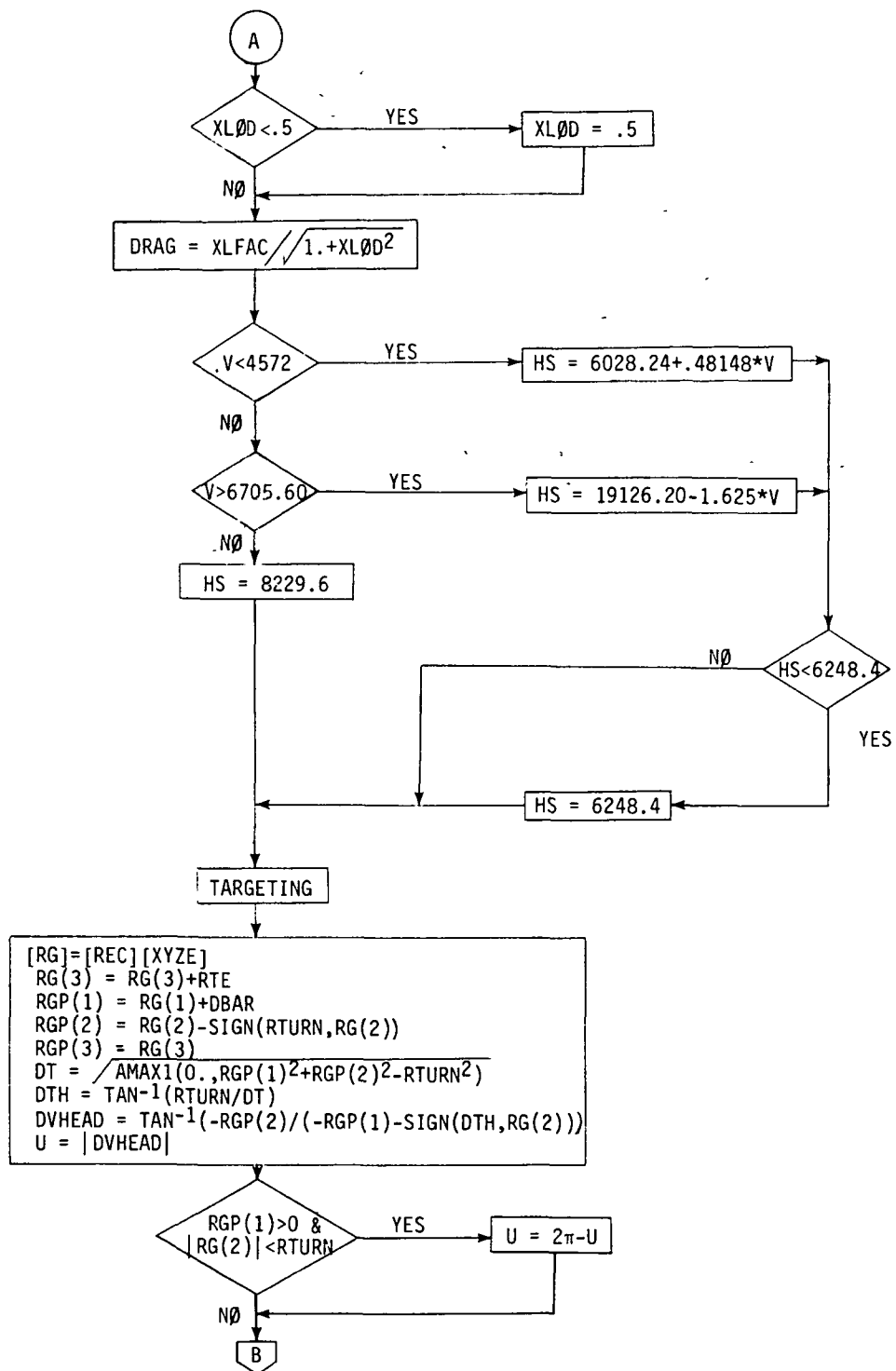
Figure 14.- Continued.
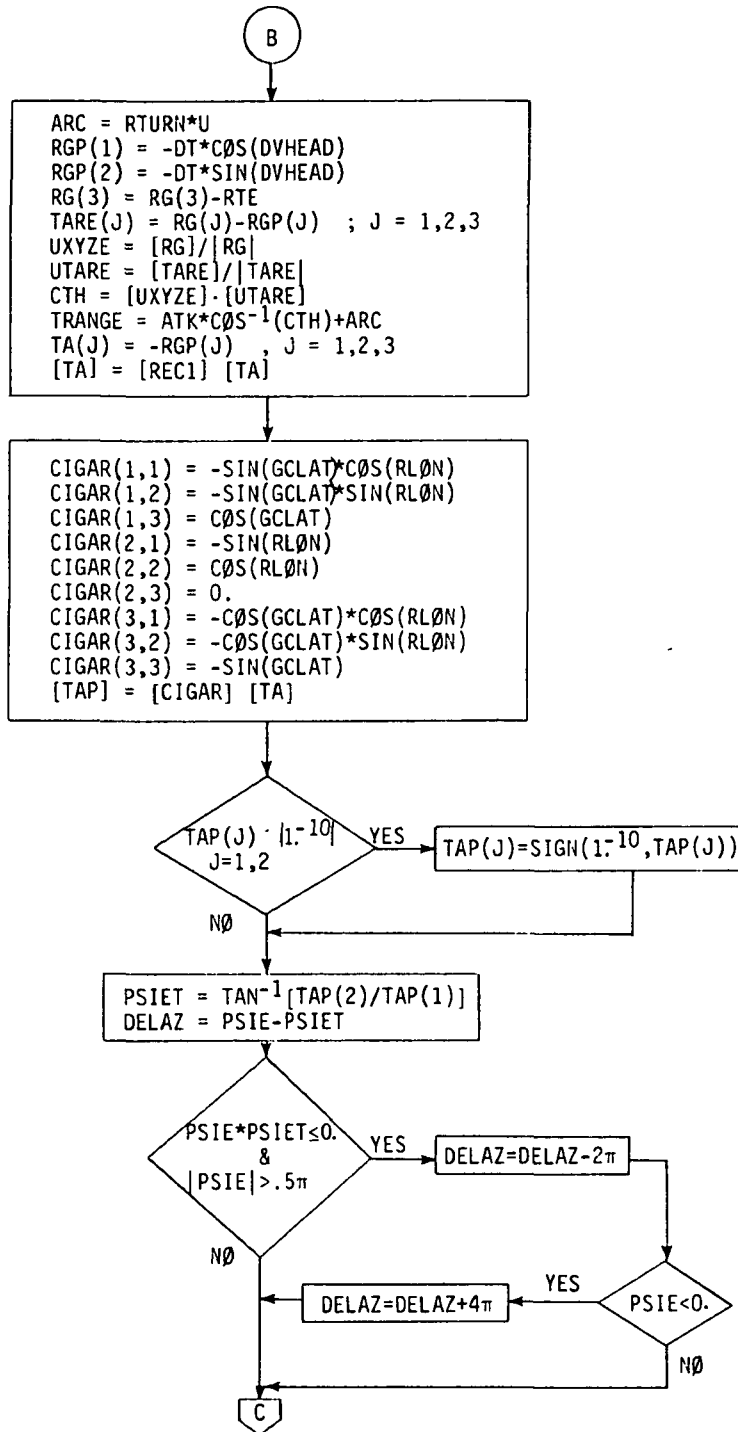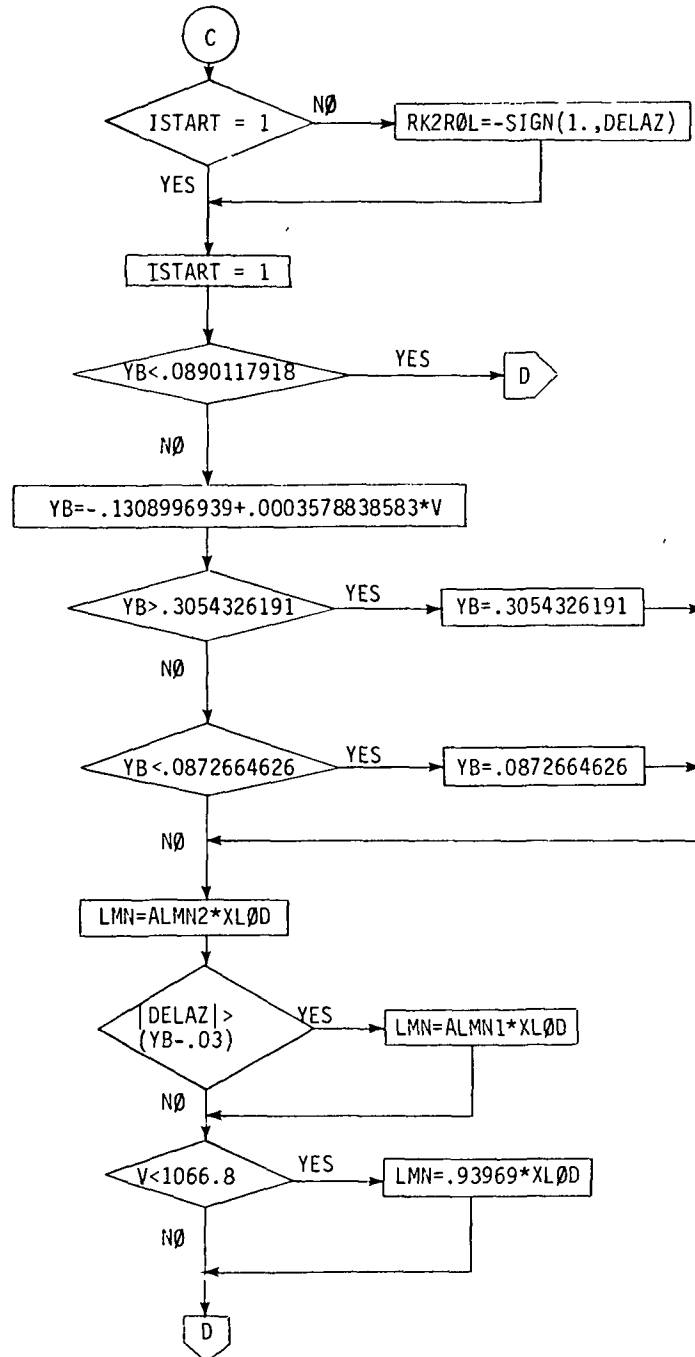
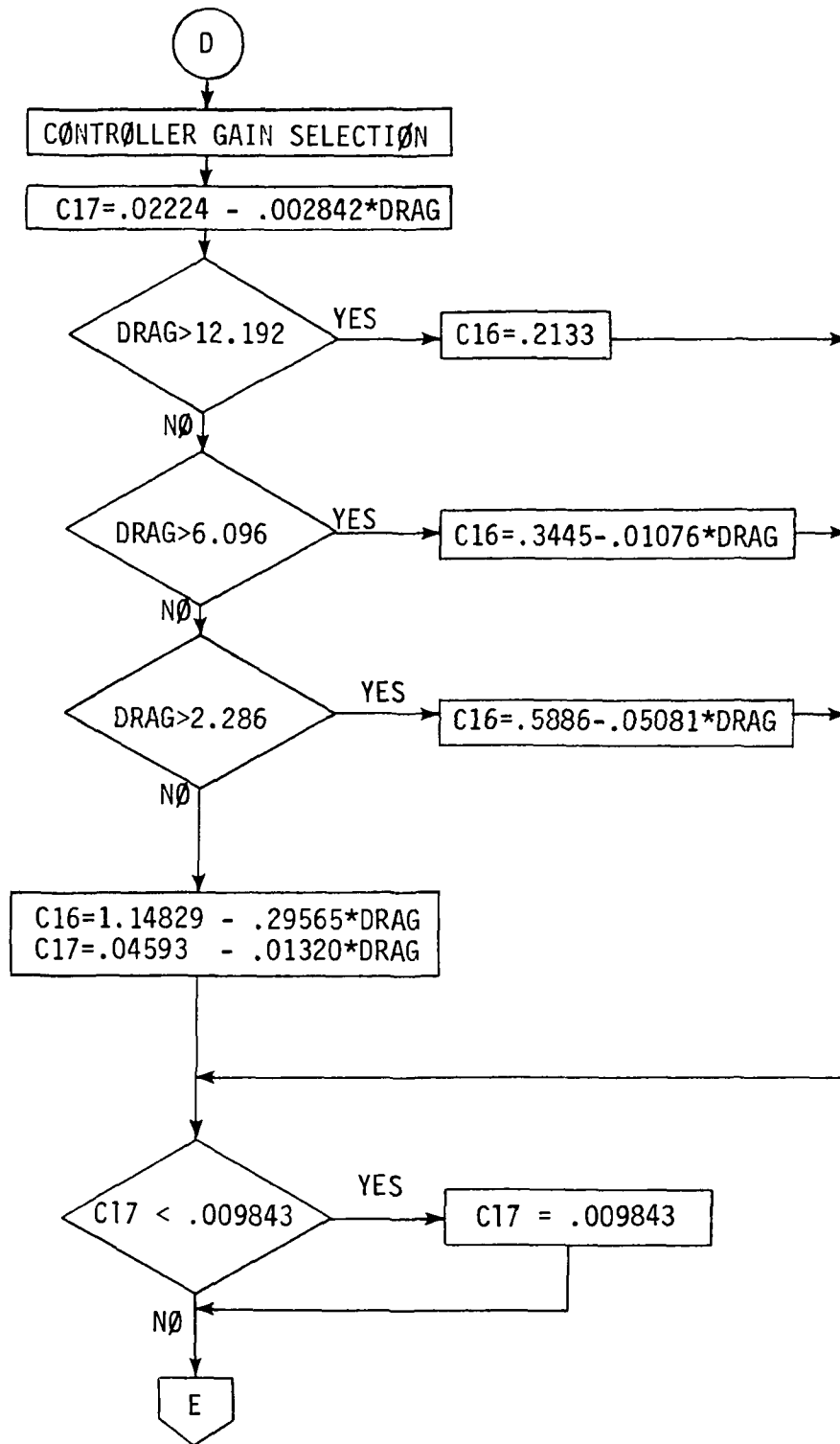Figure 14.- Continued.
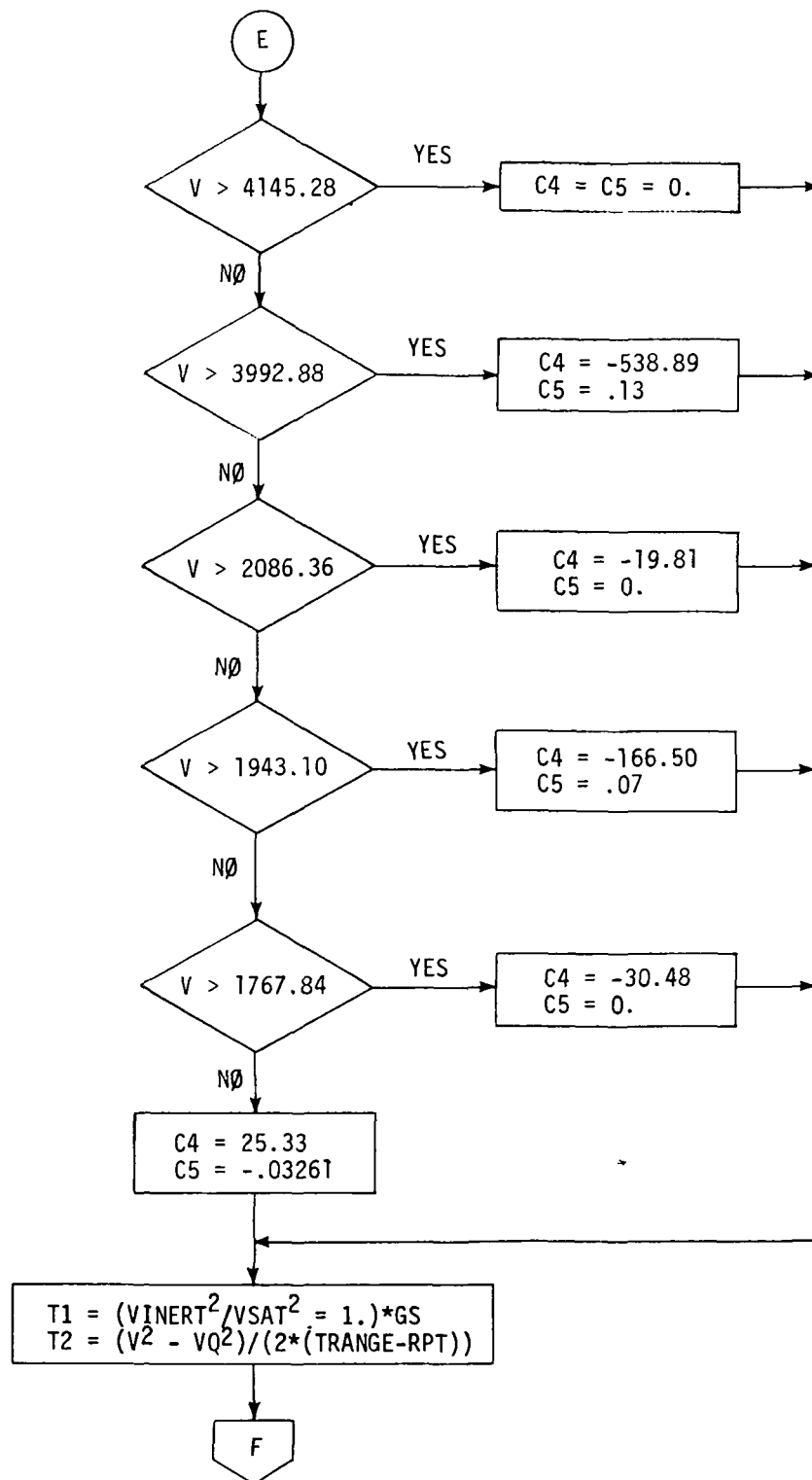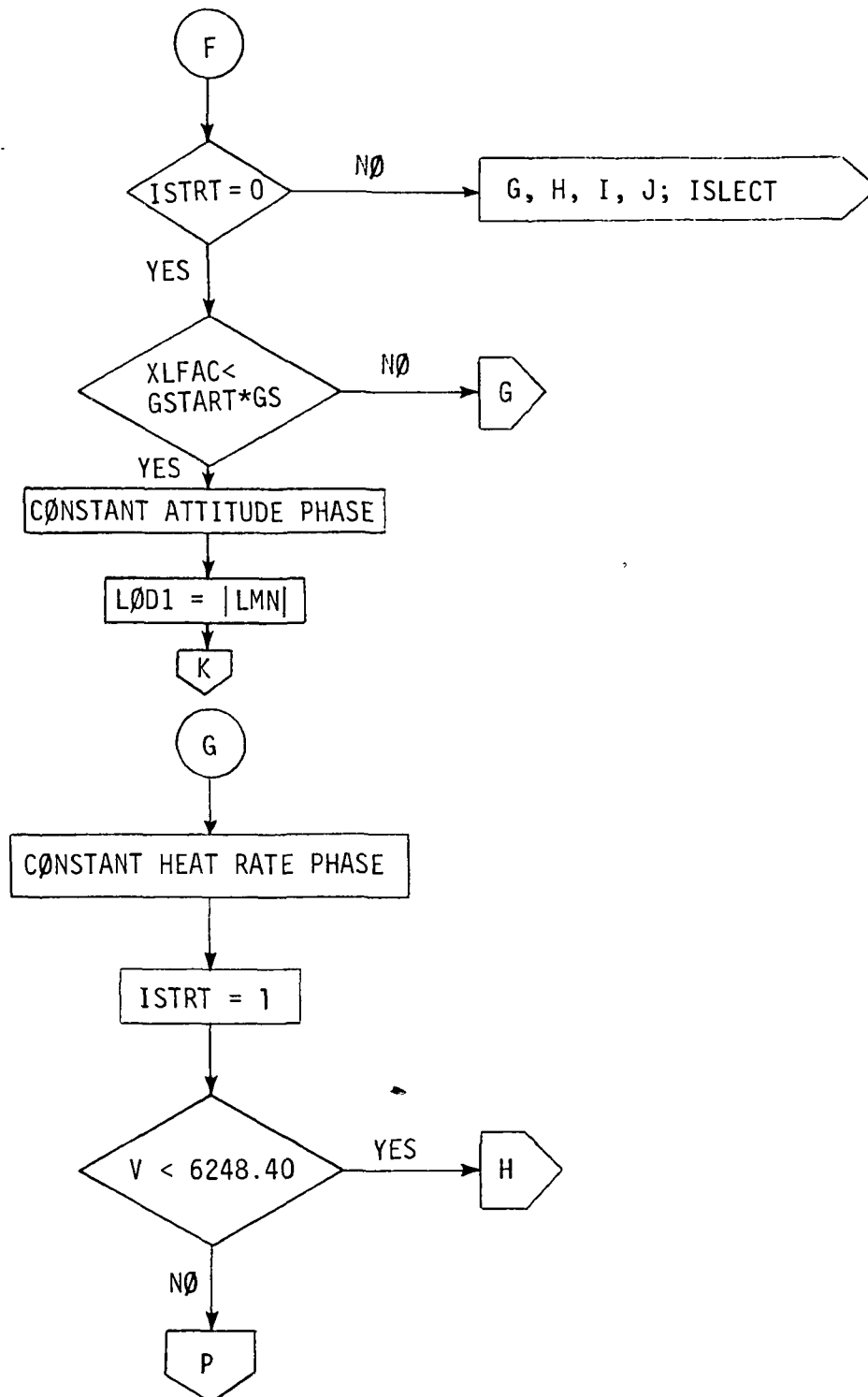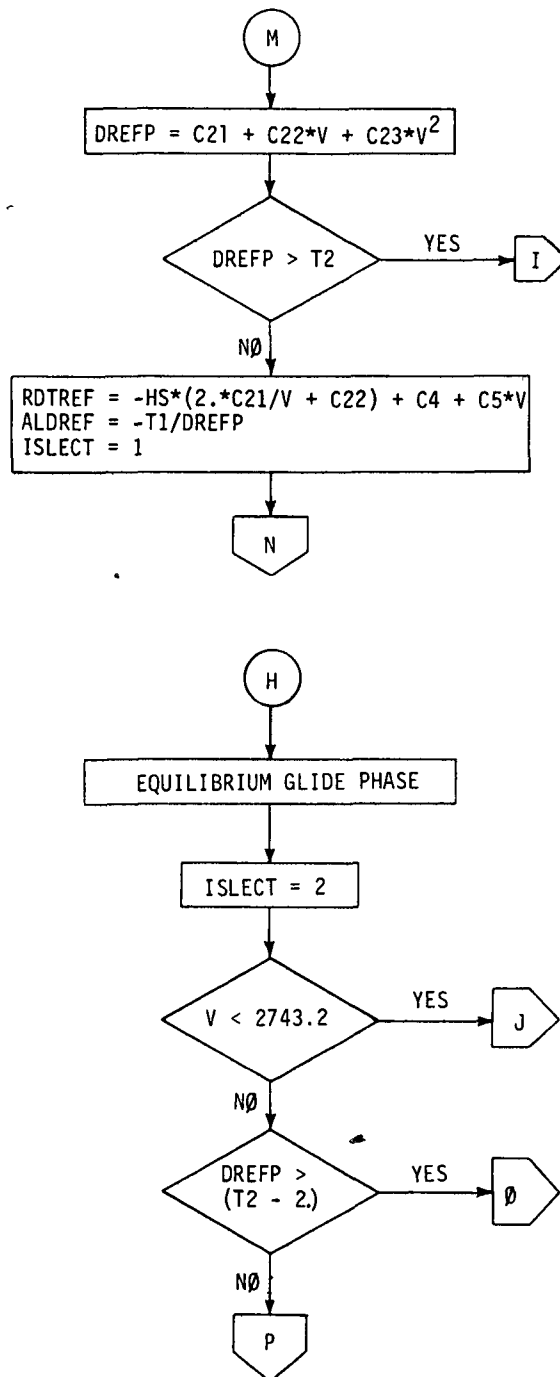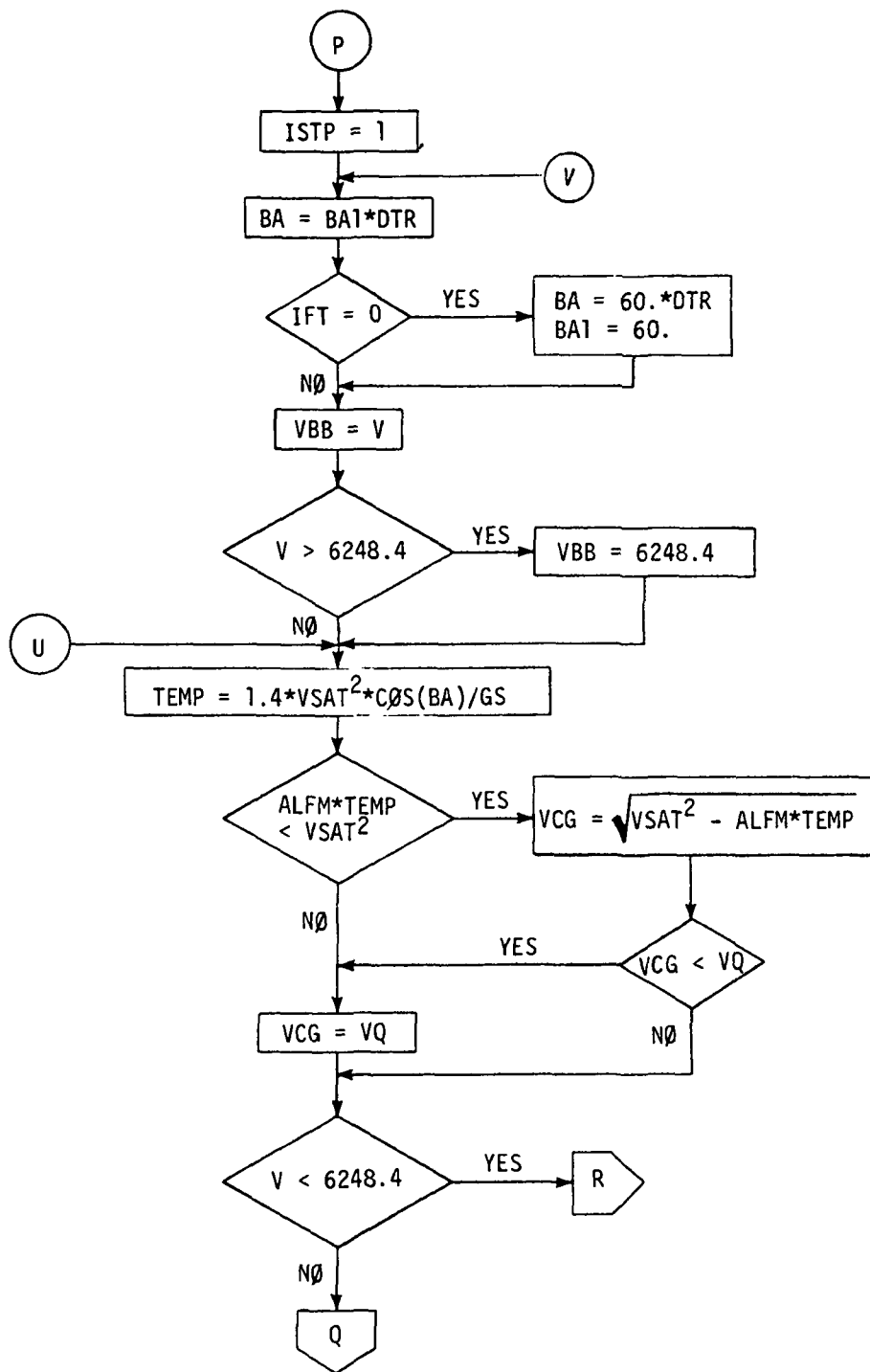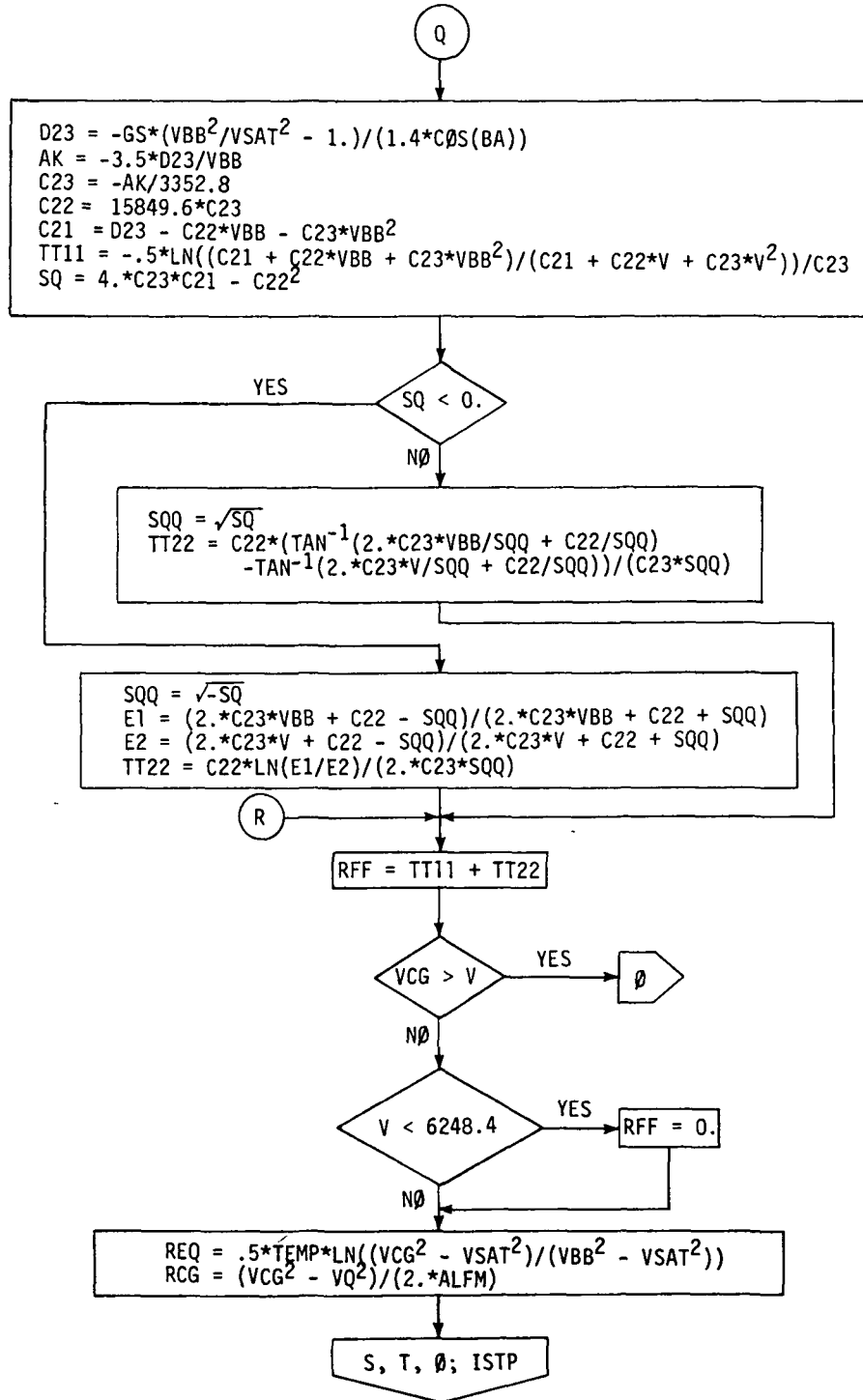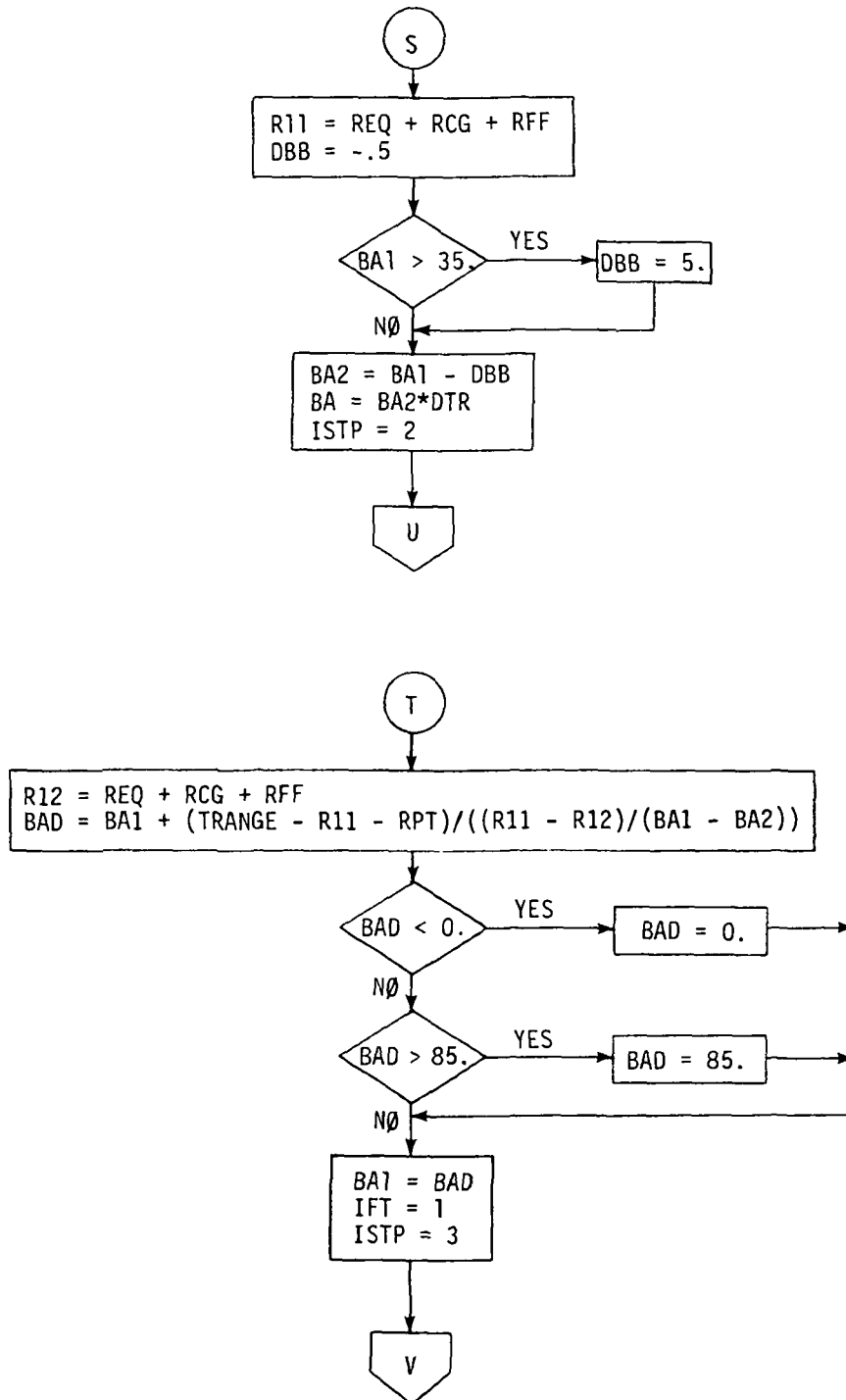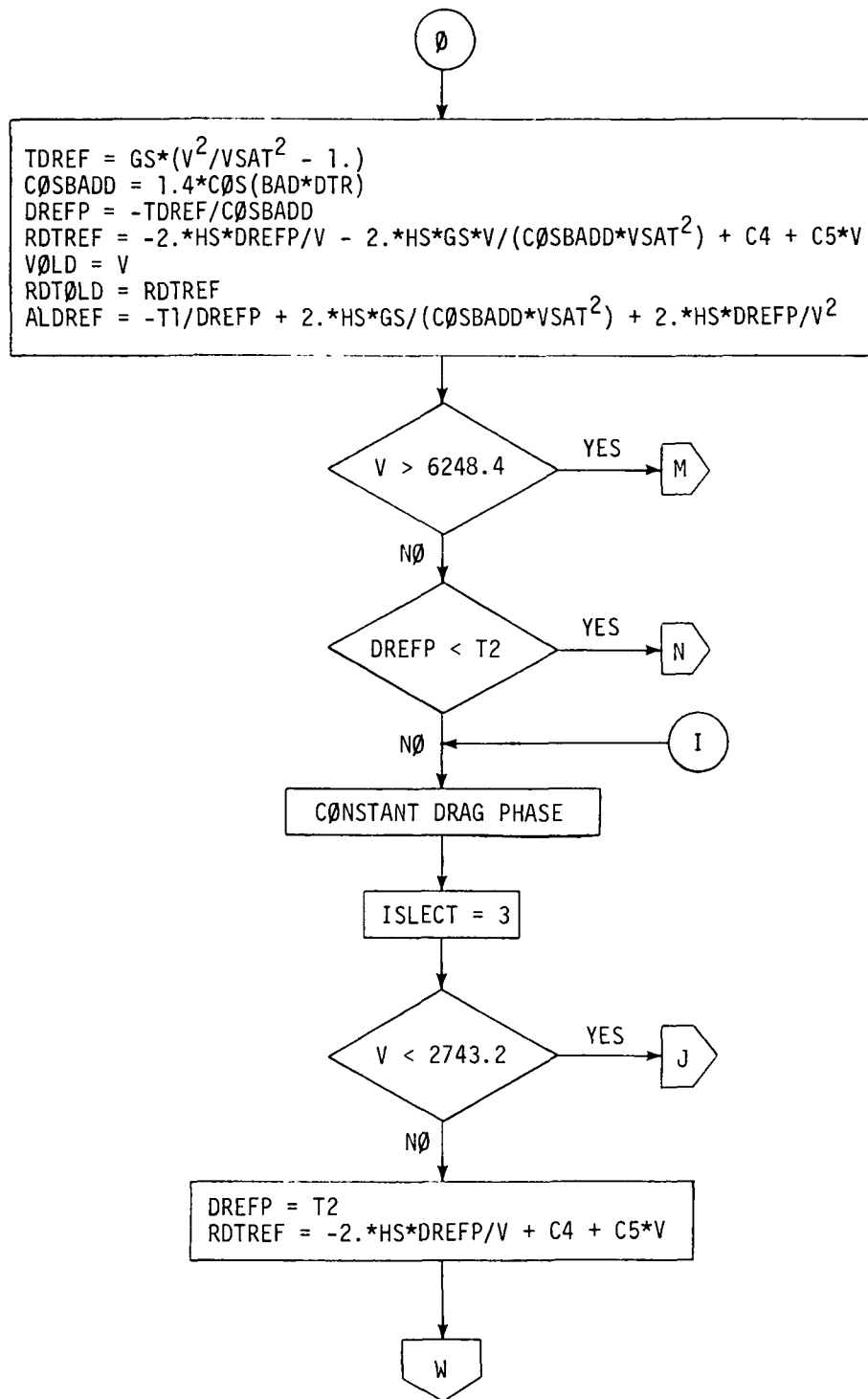
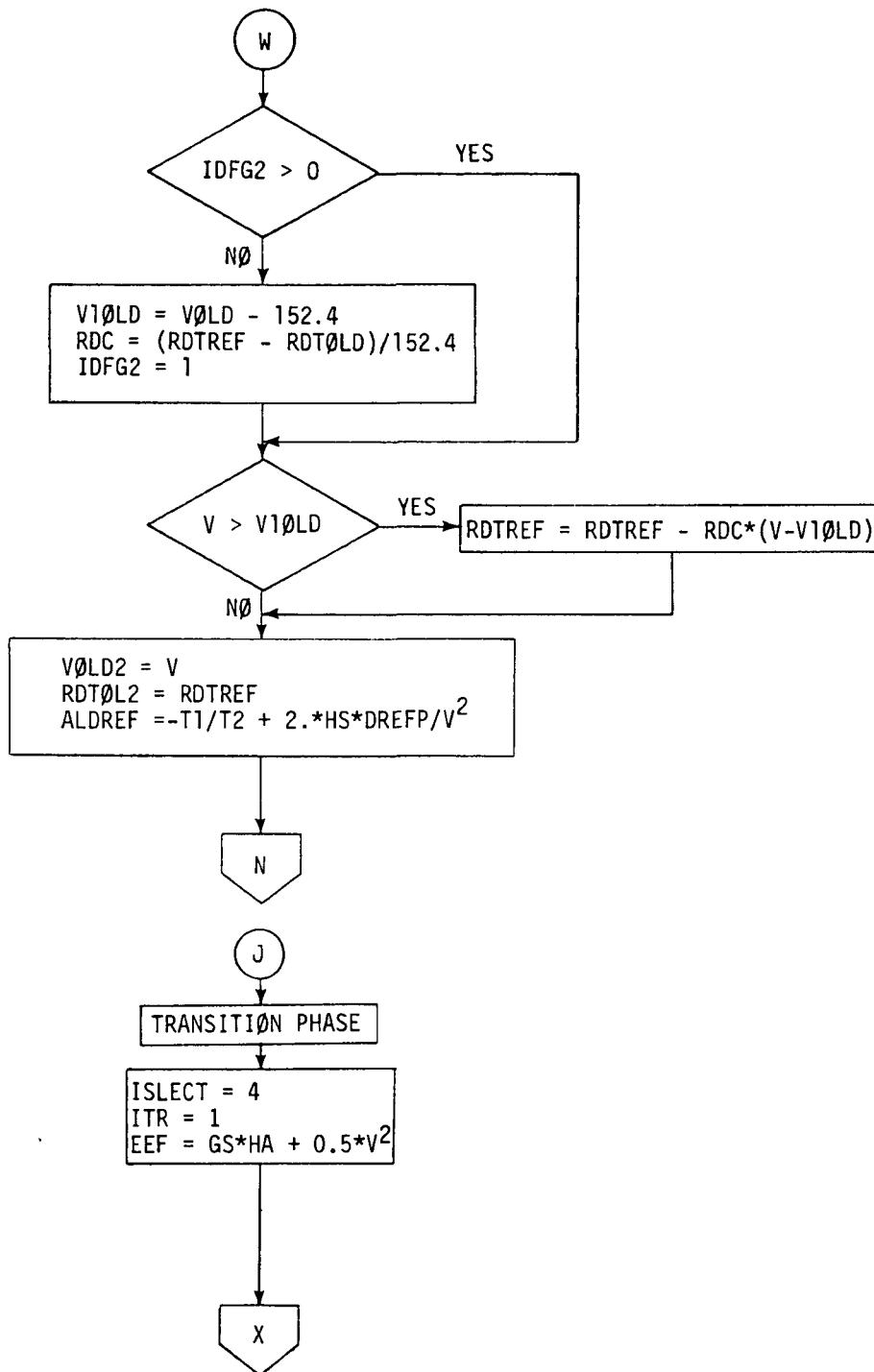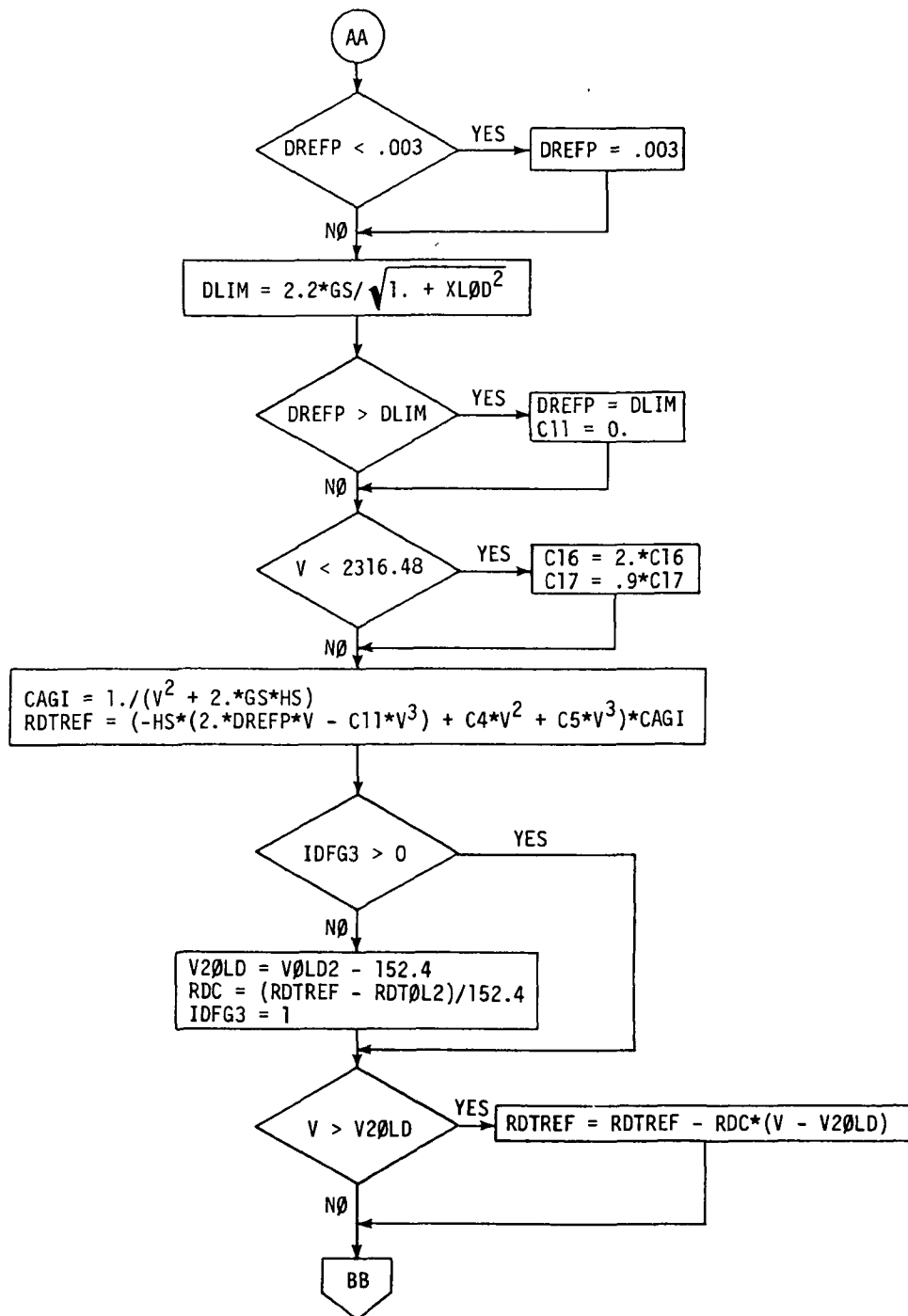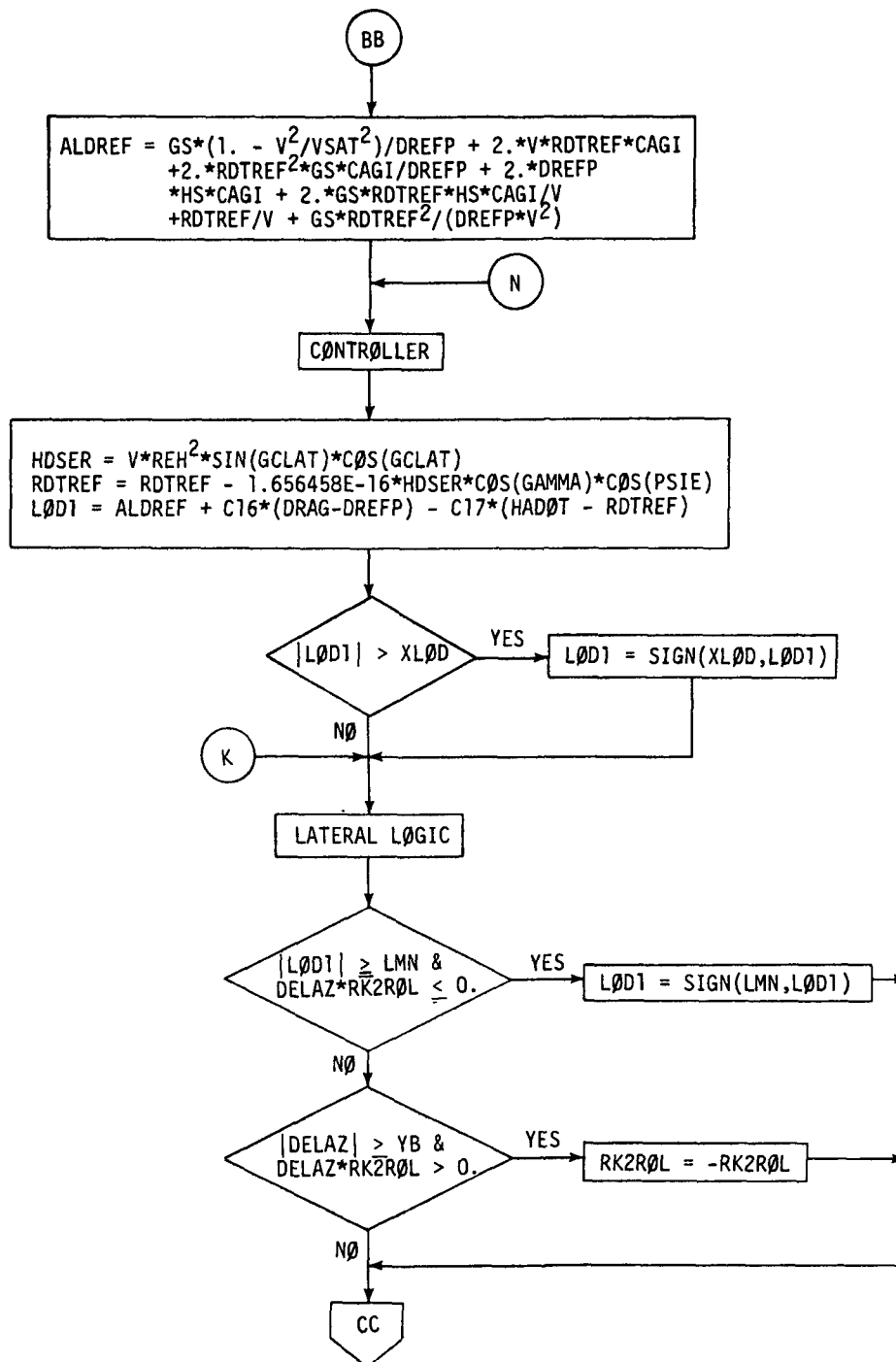Figure 14.- Continued.

Figure 14.- Continued.

Figure 14.- Continued.

Figure 14.- Continued.

$$DREFP = C21 + C22*V + C23*V^2$$

DREFP > T2 — YES → I

NØ

RDTREF = -HS*(2.*C21/V + C22) + C4 + C5*V
ALDREF = -T1/DREFP
ISLECT = 1

N

H

EQUILIBRIUM GLIDE PHASE

ISLECT = 2

V < 2743.2 — YES → J

NØ

DREFP > (T2 - 2.) — YES → Ø

NØ

P

Figure 14.- Continued.

Figure 14.- Continued.

Figure 14.- Continued.

Figure 14.- Continued.

$$TDREF = GS*(V^2/VSAT^2 - 1.)$$
$$C\emptyset SBADD = 1.4*C\emptyset S(BAD*DTR)$$
$$DREFP = -TDREF/C\emptyset SBADD$$
$$RDTREF = -2.*HS*DREFP/V - 2.*HS*GS*V/(C\emptyset SBADD*VSAT^2) + C4 + C5*V$$
$$V\emptyset LD = V$$
$$RDT\emptyset LD = RDTREF$$
$$ALDREF = -T1/DREFP + 2.*HS*GS/(C\emptyset SBADD*VSAT^2) + 2.*HS*DREFP/V^2$$

V > 6248.4   YES → M

NØ

DREFP < T2   YES → N

NØ   ← I

CØNSTANT DRAG PHASE

ISLECT = 3

V < 2743.2   YES → J

NØ

$$DREFP = T2$$
$$RDTREF = -2.*HS*DREFP/V + C4 + C5*V$$

W

Figure 14.- Continued.

Figure 14.- Continued.

Figure 14.- Continued.

Figure 14.- Continued.

Figure 14.- Continued.
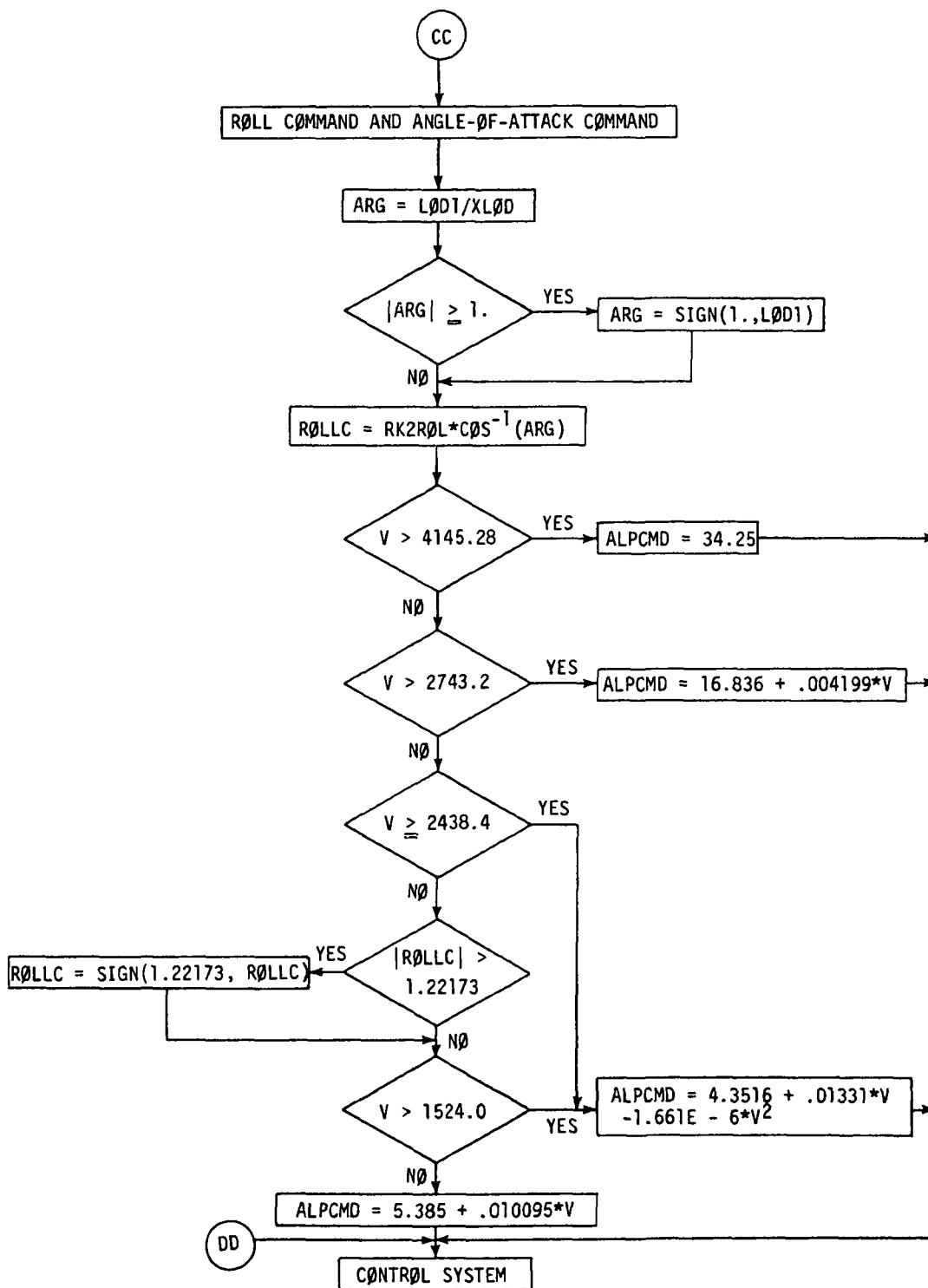
Figure 14.- Concluded.

Body-flap δ_{BF} schedule

Forward center of gravity δ_{BF} = -11.7°
Aft center of gravity δ_{BF} = 16.3°

Speed-brake δ_{SB} schedule
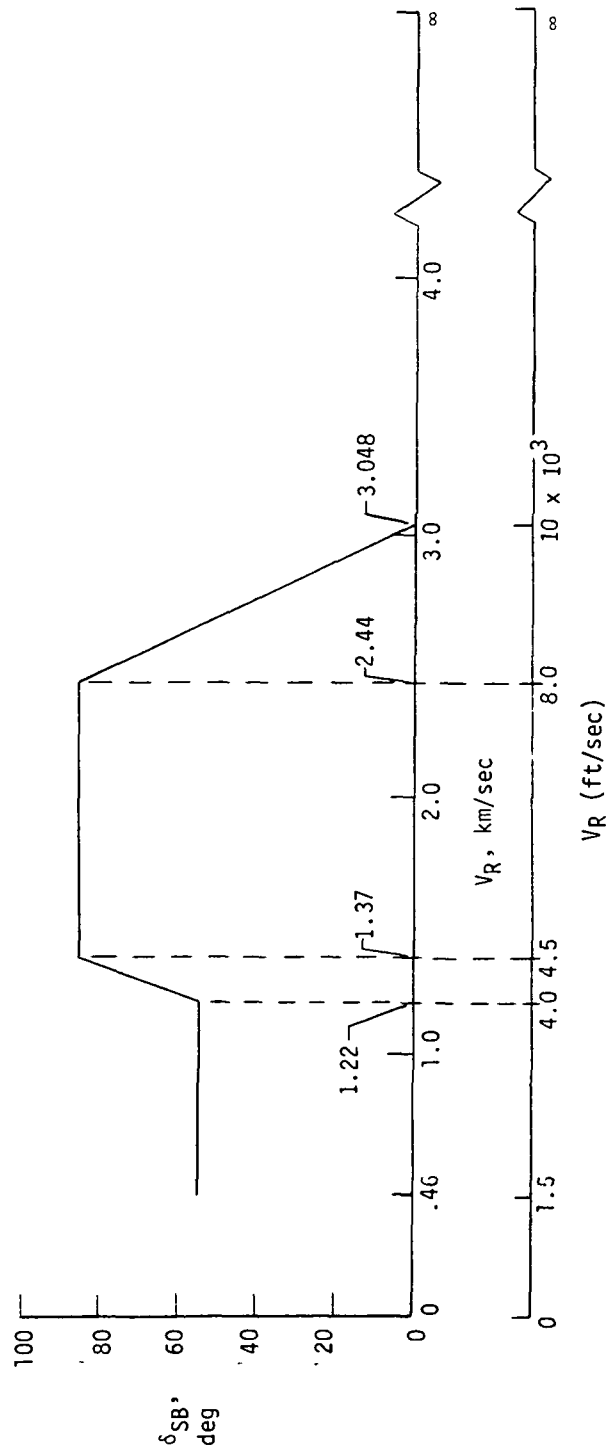
Figure 15.- Body-flap and speed-brake schedules.
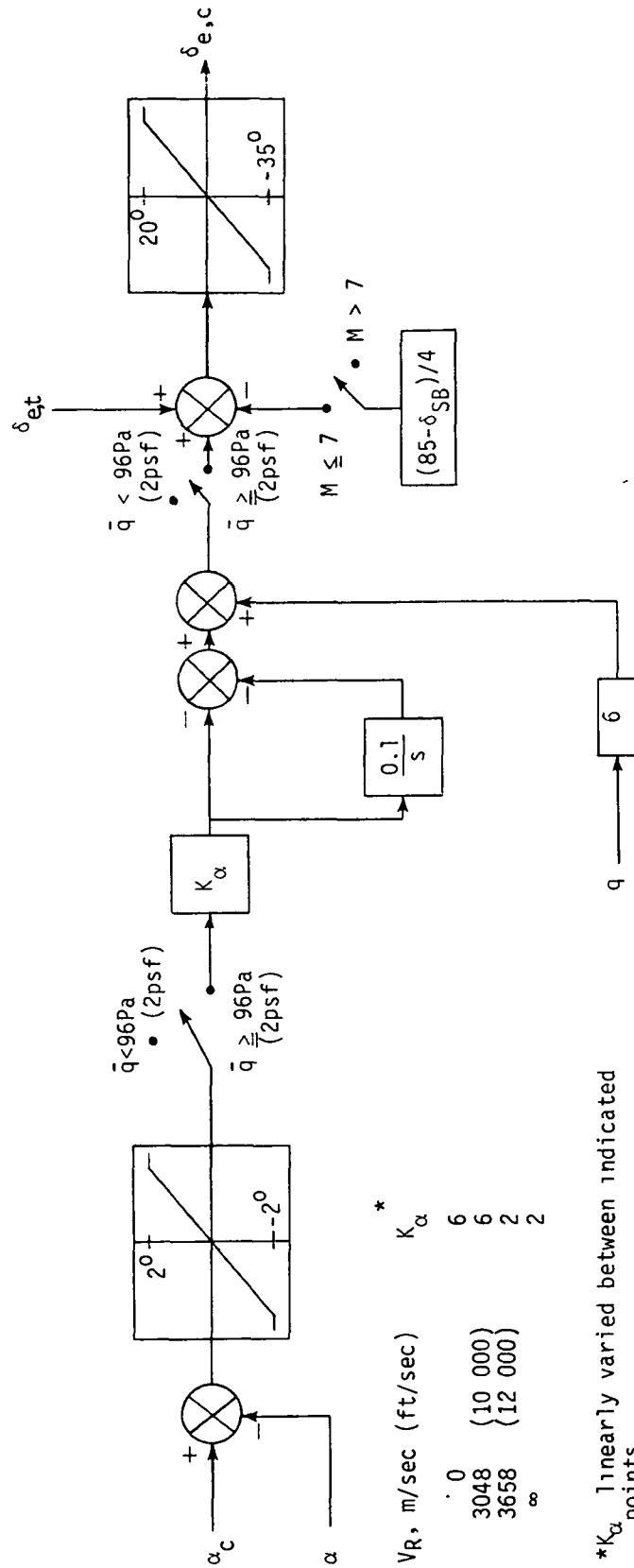
Figure 16.— Elevator command block diagram.

73
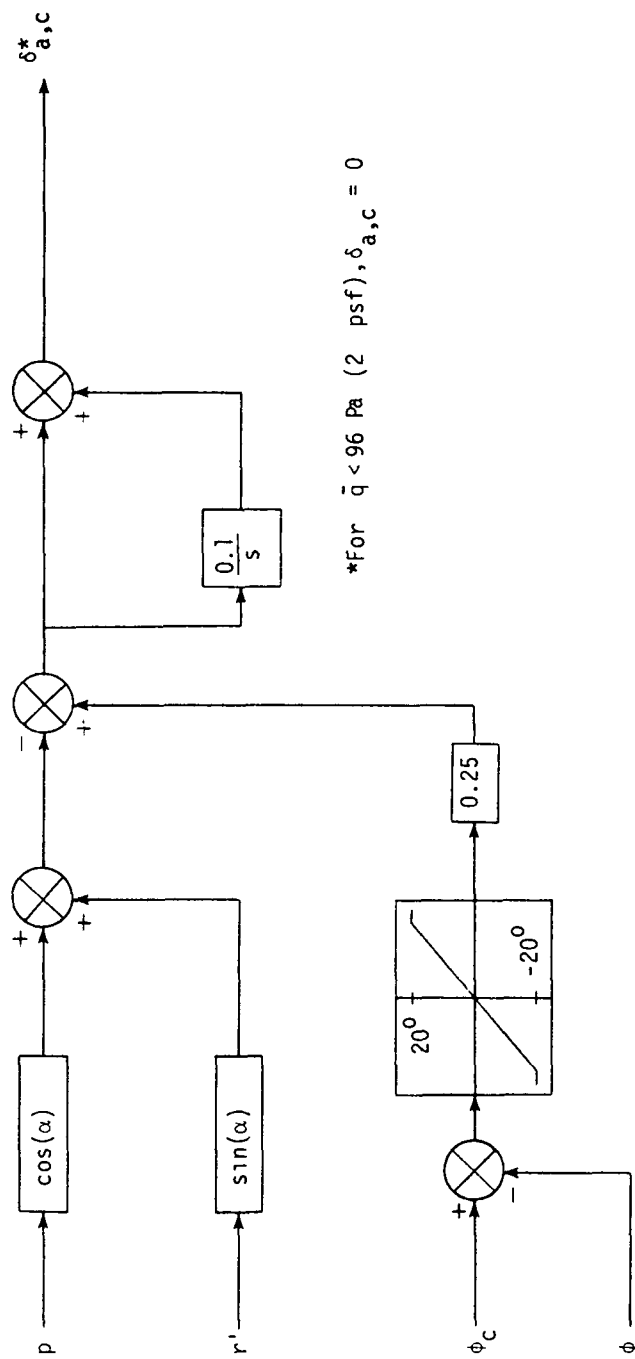
(a) α ≦ 18° and M ≦ 5.

Figure 17.- Aileron command block diagram.

(b) $\alpha > 18^\circ$ or $M > 5$.
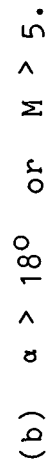
Figure 17.- Concluded.
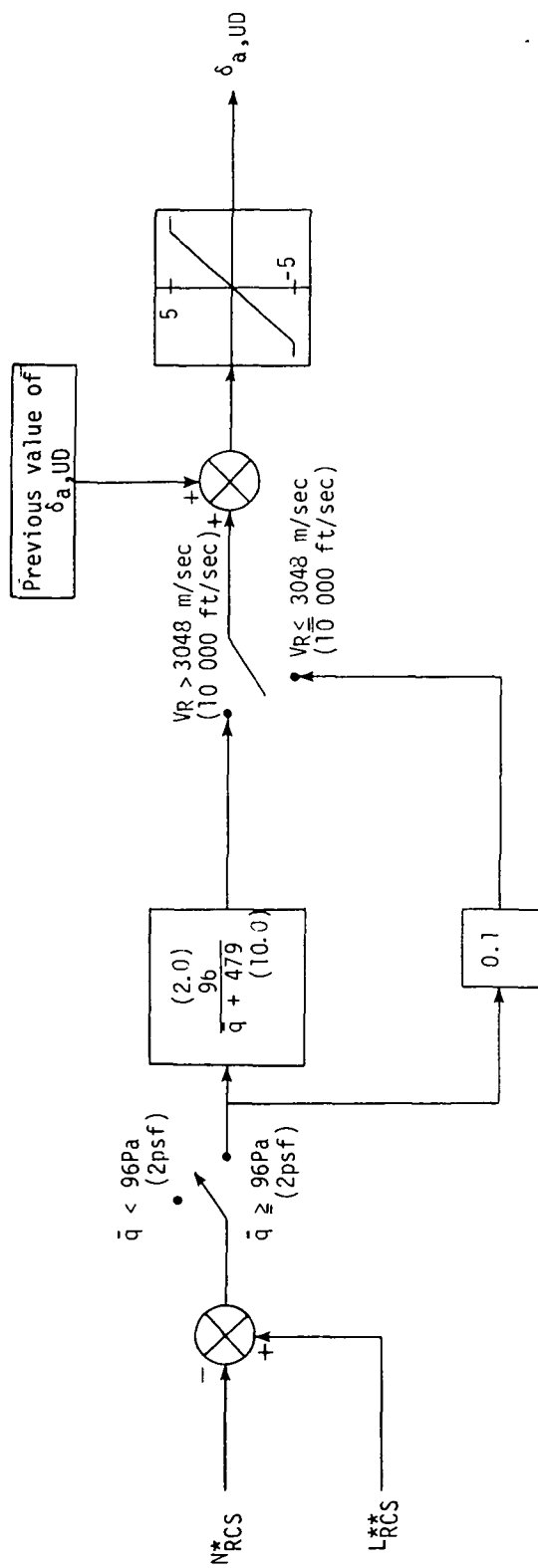
Figure 18.- Up-down counter block diagram.

*Number of yaw jets that came on (+ for positive jet, - for negative jet).

**Number of roll jets that came on (+ for positive jet, - for negative jet).

76
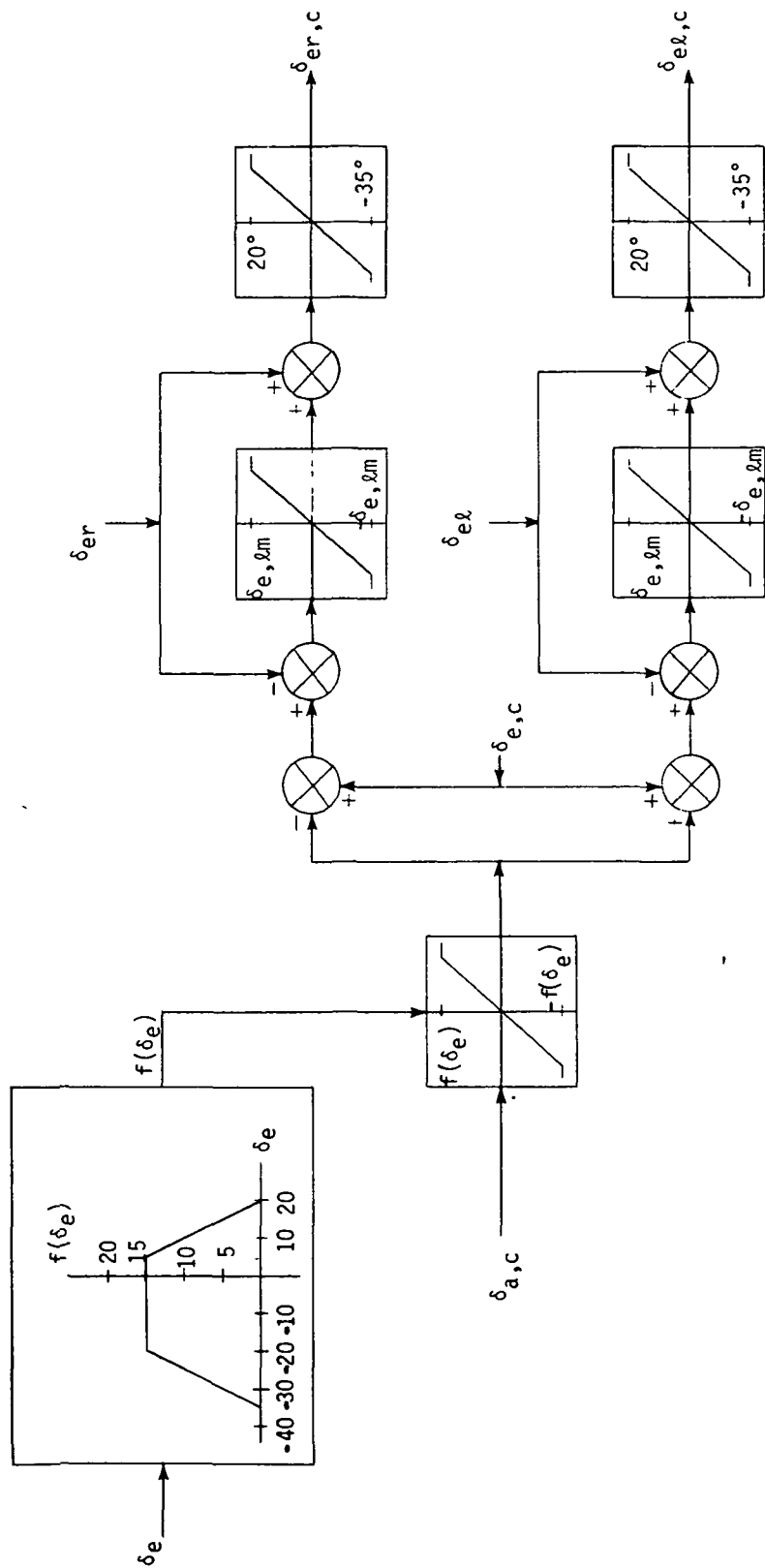
Figure 19.- Right and left elevon panel commands.
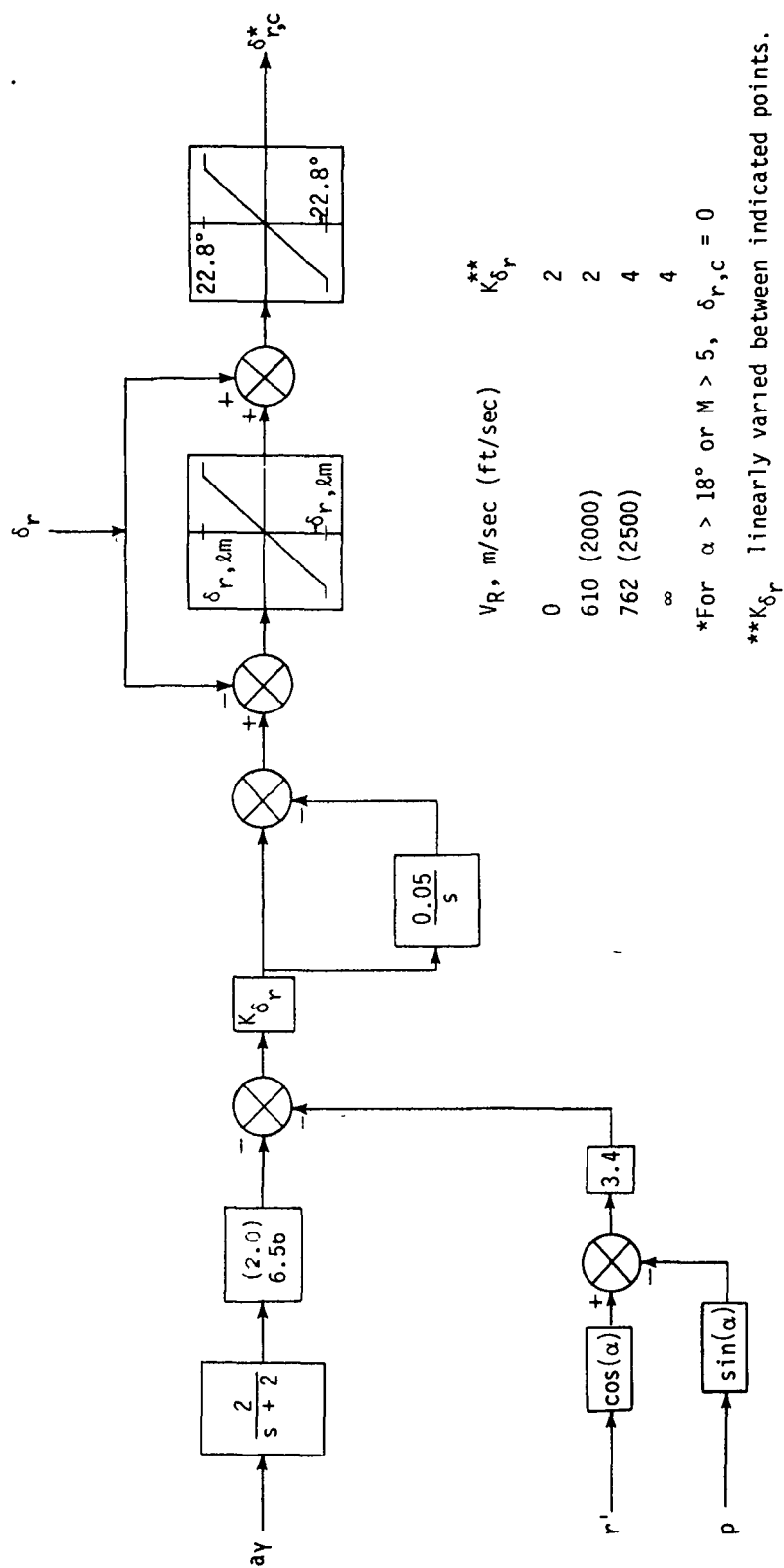
Figure 20.- Rudder command block diagram. Numbers in parentheses are in U.S. Customary Units.
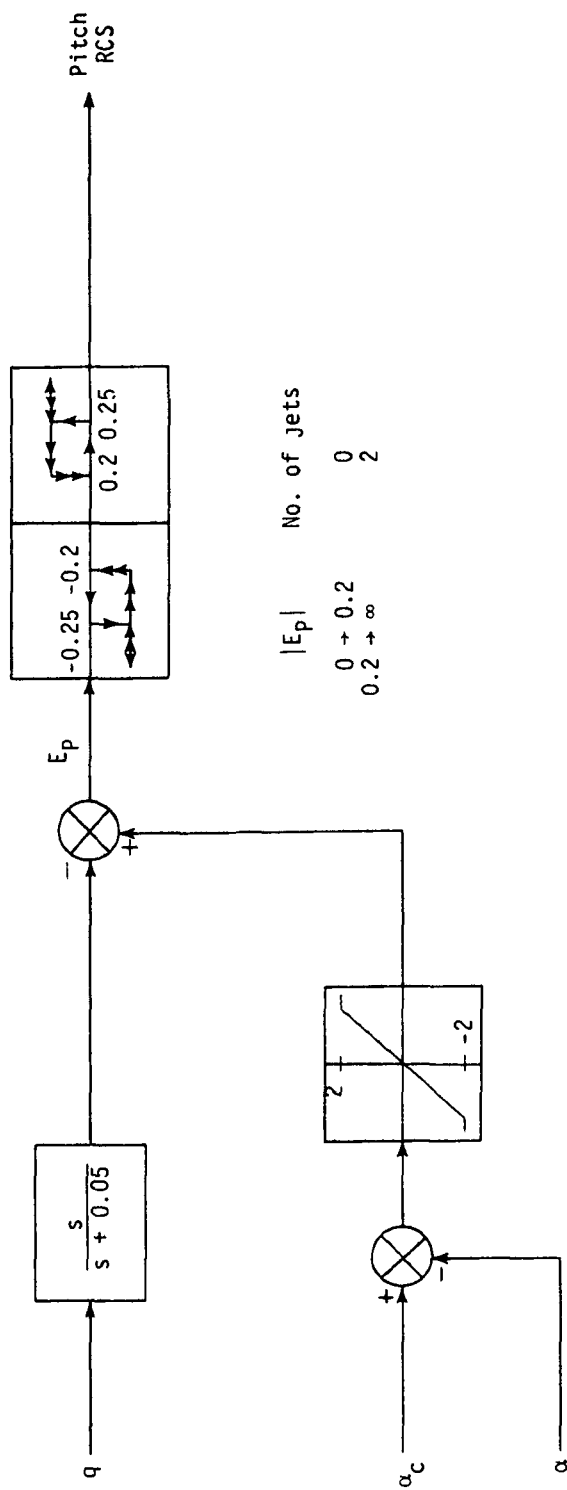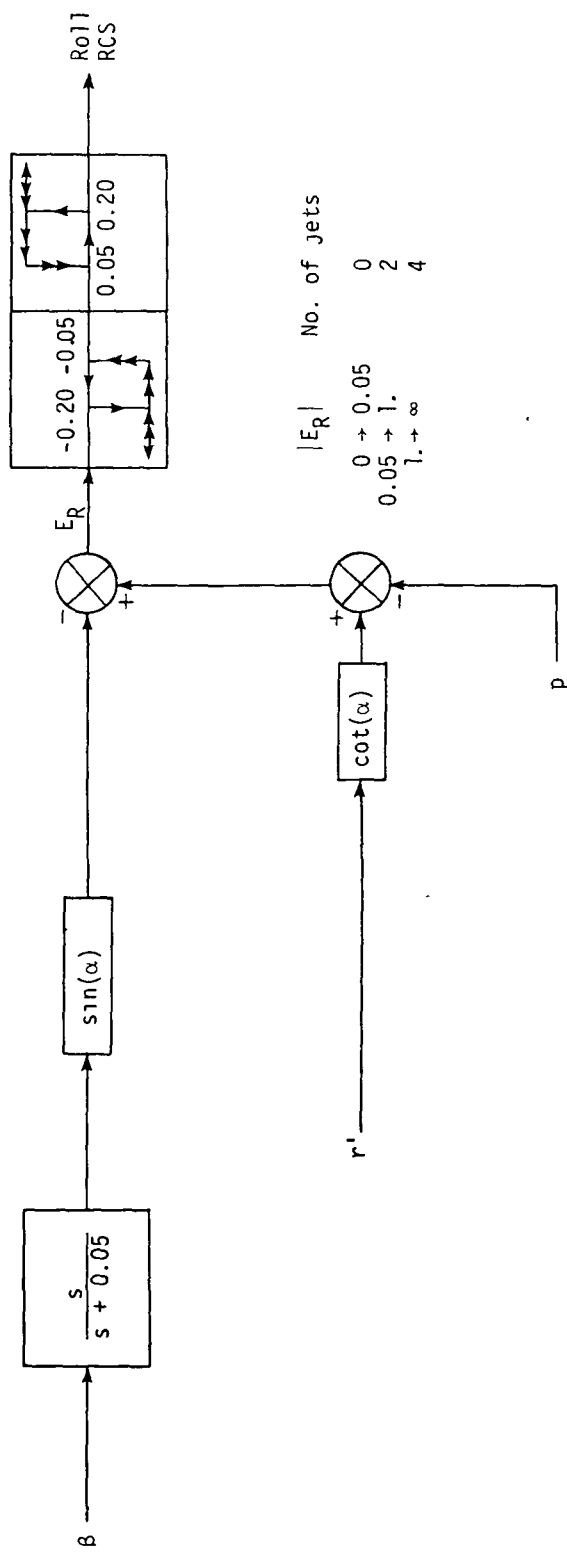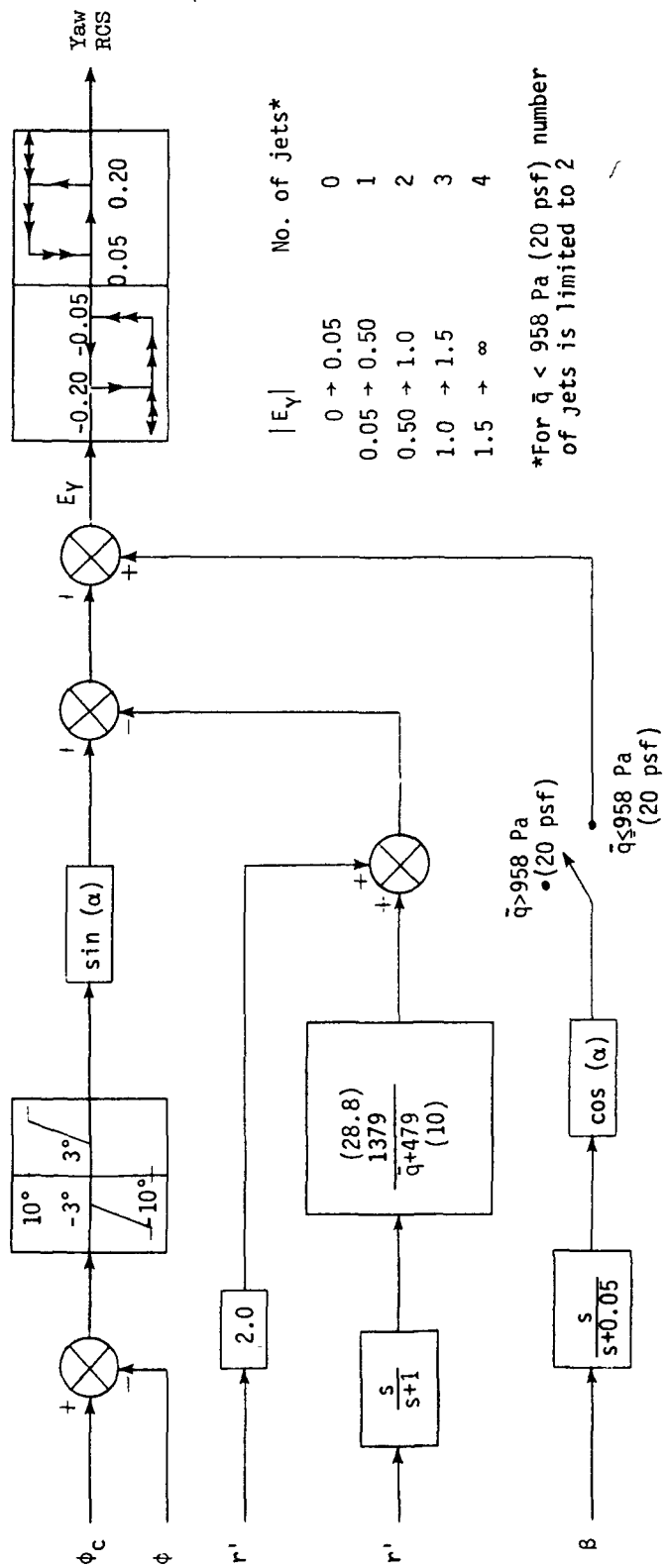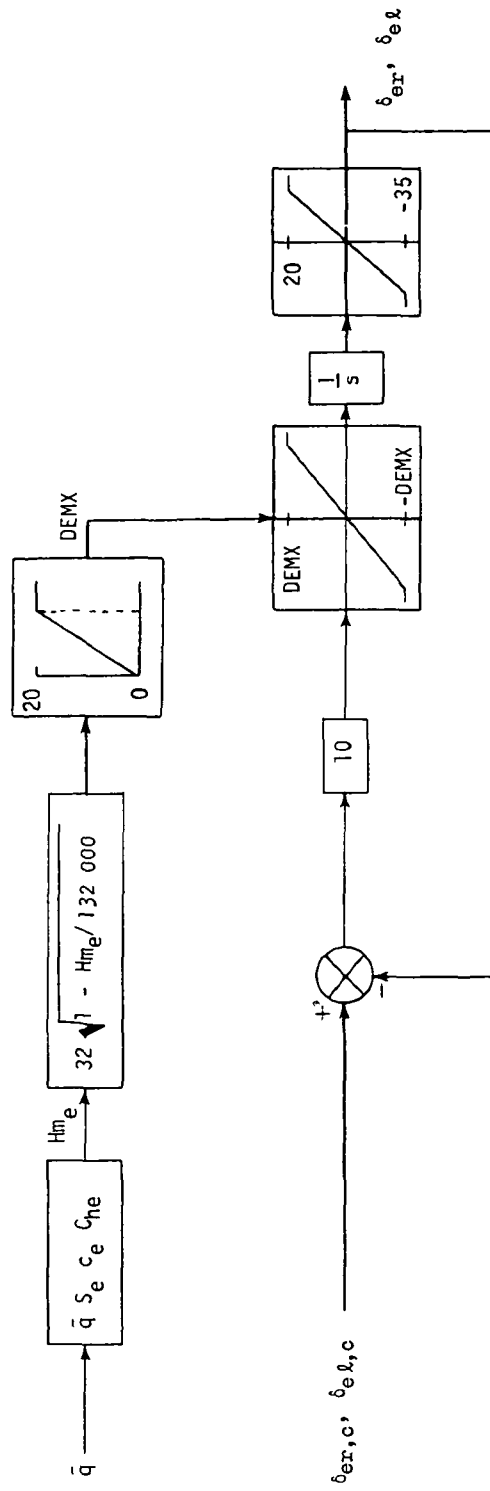
Figure 21.— Pitch RCS error-signal block diagram.

Figure 22.— Roll RCS error-signal block diagram.

(a) $\alpha \leqq 18^\circ$ and $M \leqq 5$.

Figure 23.— Yaw RCS error-signal block diagram.

81

(b) $\alpha > 18°$ or $M > 5$.

Figure 23.- Concluded.

(a) Elevon.

Figure 24.- Actuator block diagrams.

(b) Rudder.

Figure 24.- Concluded.

*"The aeronautical and space activities of the United States shall be
conducted so as to contribute . . to the expansion of human knowl-
edge of phenomena in the atmosphere and space The Administration
shall provide for the widest practicable and appropriate dissemination
of information concerning its activities and the results thereof"*
—NATIONAL AERONAUTICS AND SPACE ACT OF 1958

NASA SCIENTIFIC AND TECHNICAL PUBLICATIONS

TECHNICAL REPORTS Scientific and technical information considered important, complete, and a lasting contribution to existing knowledge.

TECHNICAL NOTES Information less broad in scope but nevertheless of importance as a contribution to existing knowledge

TECHNICAL MEMORANDUMS Information receiving limited distribution because of preliminary data, security classification, or other reasons Also includes conference proceedings with either limited or unlimited distribution.

CONTRACTOR REPORTS Scientific and technical information generated under a NASA contract or grant and considered an important contribution to existing knowledge.

TECHNICAL TRANSLATIONS Information published in a foreign language considered to merit NASA distribution in English

SPECIAL PUBLICATIONS Information derived from or of value to NASA activities. Publications include final reports of major projects, monographs, data compilations, handbooks, sourcebooks, and special bibliographies

TECHNOLOGY UTILIZATION PUBLICATIONS Information on technology used by NASA that may be of particular interest in commercial and other non-aerospace applications Publications include Tech Briefs, Technology Utilization Reports and Technology Surveys

Details on the availability of these publications may be obtained from:

SCIENTIFIC AND TECHNICAL INFORMATION OFFICE

NATIONAL AERONAUTICS AND SPACE ADMINISTRATION
Washington, D.C. 20546